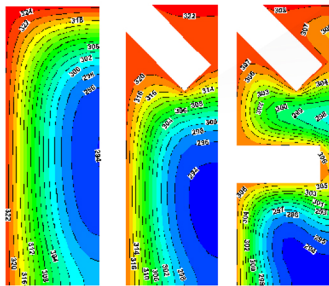
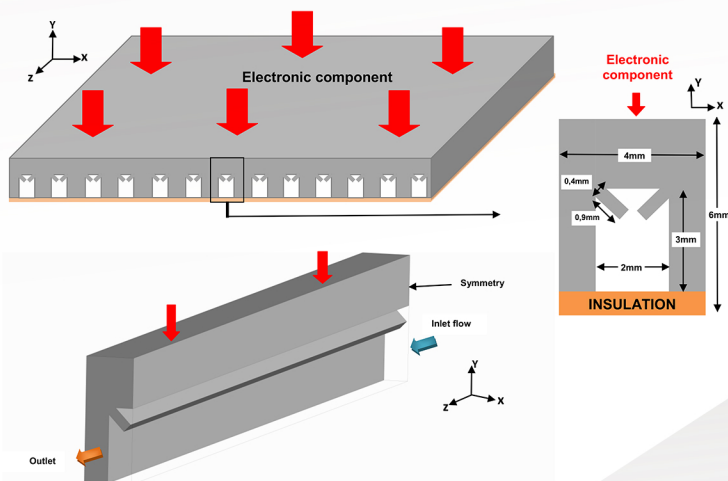


Mechanical Engineering Technologies and Applications



Editor:
Zied Driss

Bentham Books

Mechanical Engineering Technologies and Applications

(Volume 2)

Edited by

Zied Driss

Laboratory of Electromechanical Systems (LASEM)

National School of Engineers of Sfax (ENIS)

University of Sfax (US)

Sfax, Tunisia

Mechanical Engineering Technologies and Applications

(Volume 2)

Editor: Zied Driss

ISSN (Online): 2811-0455

ISSN (Print): 2811-0463

ISBN (Online): 978-981-5124-12-5

ISBN (Print): 978-981-5124-13-2

ISBN (Paperback): 978-981-5124-14-9

© 2023, Bentham Books imprint.

Published by Bentham Science Publishers Pte. Ltd. Singapore. All Rights Reserved.

First published in 2023.

BENTHAM SCIENCE PUBLISHERS LTD.

End User License Agreement (for non-institutional, personal use)

This is an agreement between you and Bentham Science Publishers Ltd. Please read this License Agreement carefully before using the ebook/echapter/ejournal (“**Work**”). Your use of the Work constitutes your agreement to the terms and conditions set forth in this License Agreement. If you do not agree to these terms and conditions then you should not use the Work.

Bentham Science Publishers agrees to grant you a non-exclusive, non-transferable limited license to use the Work subject to and in accordance with the following terms and conditions. This License Agreement is for non-library, personal use only. For a library / institutional / multi user license in respect of the Work, please contact: permission@benthamscience.net.

Usage Rules:

1. All rights reserved: The Work is the subject of copyright and Bentham Science Publishers either owns the Work (and the copyright in it) or is licensed to distribute the Work. You shall not copy, reproduce, modify, remove, delete, augment, add to, publish, transmit, sell, resell, create derivative works from, or in any way exploit the Work or make the Work available for others to do any of the same, in any form or by any means, in whole or in part, in each case without the prior written permission of Bentham Science Publishers, unless stated otherwise in this License Agreement.
2. You may download a copy of the Work on one occasion to one personal computer (including tablet, laptop, desktop, or other such devices). You may make one back-up copy of the Work to avoid losing it.
3. The unauthorised use or distribution of copyrighted or other proprietary content is illegal and could subject you to liability for substantial money damages. You will be liable for any damage resulting from your misuse of the Work or any violation of this License Agreement, including any infringement by you of copyrights or proprietary rights.

Disclaimer:

Bentham Science Publishers does not guarantee that the information in the Work is error-free, or warrant that it will meet your requirements or that access to the Work will be uninterrupted or error-free. The Work is provided "as is" without warranty of any kind, either express or implied or statutory, including, without limitation, implied warranties of merchantability and fitness for a particular purpose. The entire risk as to the results and performance of the Work is assumed by you. No responsibility is assumed by Bentham Science Publishers, its staff, editors and/or authors for any injury and/or damage to persons or property as a matter of products liability, negligence or otherwise, or from any use or operation of any methods, products instruction, advertisements or ideas contained in the Work.

Limitation of Liability:

In no event will Bentham Science Publishers, its staff, editors and/or authors, be liable for any damages, including, without limitation, special, incidental and/or consequential damages and/or damages for lost data and/or profits arising out of (whether directly or indirectly) the use or inability to use the Work. The entire liability of Bentham Science Publishers shall be limited to the amount actually paid by you for the Work.

General:

1. Any dispute or claim arising out of or in connection with this License Agreement or the Work (including non-contractual disputes or claims) will be governed by and construed in accordance with the laws of Singapore. Each party agrees that the courts of the state of Singapore shall have exclusive jurisdiction to settle any dispute or claim arising out of or in connection with this License Agreement or the Work (including non-contractual disputes or claims).
2. Your rights under this License Agreement will automatically terminate without notice and without the

need for a court order if at any point you breach any terms of this License Agreement. In no event will any delay or failure by Bentham Science Publishers in enforcing your compliance with this License Agreement constitute a waiver of any of its rights.

3. You acknowledge that you have read this License Agreement, and agree to be bound by its terms and conditions. To the extent that any other terms and conditions presented on any website of Bentham Science Publishers conflict with, or are inconsistent with, the terms and conditions set out in this License Agreement, you acknowledge that the terms and conditions set out in this License Agreement shall prevail.

Bentham Science Publishers Pte. Ltd.

80 Robinson Road #02-00

Singapore 068898

Singapore

Email: subscriptions@benthamscience.net



CONTENTS

PREFACE	i
LIST OF CONTRIBUTORS	iii
CHAPTER 1 NUMERICAL INVESTIGATION OF TURBULENT SLOT JETS WITH VARIOUS NANOPARTICLES SHAPES	1
<i>Bouziane Boudraa and Rachid Bessaih</i>	
INTRODUCTION	1
GEOMETRY OF THE PROBLEM	4
Governing Equations	5
Turbulence Model	6
Nanofluid Properties	7
BOUNDARY CONDITIONS	8
Computational Model	9
Test Grid	9
RESULTS	10
Validation	10
Comparison between Single and Two-Phase Models	10
Effect of Reynolds Numbers	12
Effect of Nanoparticles Volume Friction	14
Performance Evaluation Criteria	15
CONCLUSION	16
REFERENCES	16
CHAPTER 2 THE EXPERIMENTAL STUDY ON A SWEEPING GAS MEMBRANE DISTILLATION UNIT	21
<i>Mokhless Boukhriss, Mohamed Ali Maatoug, Mahdi Timoumi and Nizar El Ouni</i>	
INTRODUCTION	21
THEORETICAL MODEL STUDY	23
Hypothesis	25
RESULTS AND DISCUSSION	25
Effect of Temperature in SGMD	25
Effect of Gas Flow in SGMD	25
Effect of Liquid Flow in the SGMD	27
CONCLUSION	28
ACKNOWLEDGEMENTS	28
REFERENCES	29
CHAPTER 3 DEVELOPMENT OF DESIGN PROCESSES FOR MULTI-SPINDLE DRILLING USING THE NEURAL NETWORK AND EXPERT SYSTEM	30
<i>Ayoub Fajraoui and Kamel Mehdi</i>	
INTRODUCTION	30
LITERATURE REVIEW	31
DESIGN METHODOLOGY	32
Application of Artificial Neural Networks	32
Knowledge Base of Expertise	33
On the Learning Algorithm of the Neural Network	34
Object-Oriented Design Support Tools	35
<i>Expert System as Decision Support System Tool</i>	35
Structure and Description of the Presented Expert System	35
IMPLEMENTATION OF THE EXPERT SYSTEM SADC BPM	37

Gear Design	37
METHODS, RULES, AND FUNCTIONS IN EXPERT SYSTEM SADBPM	40
RESULTS AND ANALYSIS	40
CONCLUSION	44
REFERENCES	45
CHAPTER 4 EXPERIMENTAL INVESTIGATION OF A NEW HYBRID SOLAR COLLECTOR (PV/T) SYSTEM	47
<i>Mohamed Fterich, Houssam Chouikhi, Hatem Bentaher and Aref Maalej</i>	
INTRODUCTION	48
COLLECTOR DESIGN AND EQUIPMENT	50
INSTRUMENTS	51
THEORY AND CALCULATION	51
RESULTS AND DISCUSSION	52
Hourly Evolution of the Various Temperatures and Solar Radiation	52
Electrical Performance of the Hybrid Solar PV/T Collector for Different Mass Flow Rates	53
Influence of Solar Radiation on the Variation of the Electrical Power for PV/T Collector ...	54
Influence of Mass Flow Rate on the Variation of Thermal Power and Electrical Power for PV/T Collector	54
The Influence of Mass Flow Rate and Solar Radiation on the Variation of Outlet Temperature for the PV/T Collector	56
Influence of the Mass Flow Rate on the Variation of Both Thermal and Electrical Efficiencies for the PV/T Collector	56
CONCLUSION	57
ACKNOWLEDGEMENTS	57
REFERENCES	58
CHAPTER 5 THEORETICAL STUDY OF THE EFFECTS OF COMBUSTION DURATION ON ENGINE PERFORMANCE	60
<i>Mohamed Brayek, Amara Ibrahim, Mohamed Ali Jemni, Ali Damak, Zied Driss and Mohamed Salah Abid</i>	
INTRODUCTION	60
SPARK IGNITION ENGINE MODELING	64
Cylinder Volume and Surface Model	64
Thermodynamic Modeling	67
Pressure and Temperature Evolution as a Function of the Crank Angle	68
Work	70
Thermal Efficiency	70
The Mean Effective Pressure	70
The Effective Torque	70
The Effective Power	71
Combustion Efficiency	71
Heat Release Model	71
Heat Loss During Combustion	72
MODELING ENGINE ON MATLAB	74
RESULTS AND DISCUSSION	75
CONCLUSION	81
REFERENCES	81
CHAPTER 6 EFFECTS OF PREHEATING TEMPERATURE AND FUEL-AIR EQUIVALENC RATIO ON POLLUTION CONTROL IN HYDRO CARBON COMBUSTION	84
<i>Rachid Renane, Rachid Allouche and Nour Abdelkader</i>	

INTRODUCTION	85
ASSUMPTIONS ON THE MODE OF COMBUSTION	85
THERMODYNAMIC EQUILIBRIUM CONDITION	88
COMPOSITION OF THE COMBUSTION PRODUCTS	89
Fuel-air Equivalence Ratio and Stoichiometry	90
ADIABATIC FLAME TEMPERATURE CALCULUS	91
Combustion for Constant Pressure	91
Enthalpy of the Reactants	92
Enthalpy of The Combustible	92
Enthalpy of Air	93
Enthalpy of Products	93
Equilibrium Equations of Dissociation Reaction [4, 23]	94
Atomic Balance in Molar Fraction	95
METHOD OF RESOLUTION	96
Combustion Temperatures Calculus using Dichotomy Method	97
RESULTS AND COMMENTS	97
Effect of Air Preheating Temperature on the Adiabatic Flame Temperature for Kerosene and Methane Combustion	98
Effect of Equivalence Ratio Φ on Adiabatic Flame Temperature for Methane Combustion	98
Effect of Equivalence Ratio Φ on Evolution of Molar Composition of Products of Combustion	99
Effect of Preheating Temperature on the Production of Pollutants for Different Fuel-air Equivalence Ratio	100
CONCLUSION	101
LIST OF ABBREVIATIONS	102
ACKNOWLEDGEMENT	103
REFERENCES	103

**CHAPTER 7 NUMERICAL STUDY OF NATURAL CONVECTION BETWEEN TWO
CONCENTRIC ELLIPSES WITH DIFFERENT SHAPES AND IMPOSED TEMPERATURES** 105

<i>Abderrahmane Horimek, Farhat Abdelmoumene and Noureddine Ait-Messaoudene</i>	
INTRODUCTION	105
DESCRIPTION OF THE PROBLEM	108
Dimensionless Governing Equation	109
Nusselt Number Calculation	110
RESOLUTION PROCEDURE	111
Validation	111
RESULTS AND DISCUSSION	113
Case of Two Concentric Circles	113
<i>Effect of Ra and Thermal Condition for $R1/R2=0.5$</i>	113
<i>Effect of the Aspect Ratio (Hydraulic Diameter)</i>	114
Case of Circle and Ellipse	118
<i>Outer Circle/Inner Horizontal Ellipse</i>	118
<i>Outer Horizontal Ellipse/Inner Circle</i>	118
<i>Outer Circle/Inner Vertical Ellipse</i>	120
<i>Outer Vertical Ellipse/Inner Circle</i>	120
Case of Two Ellipses	121
<i>Outer and Inner Horizontal Ellipses:</i>	121
<i>Outer and Inner Vertical Ellipses</i>	122
<i>Effect of the Aspect Ratio</i>	123
Nusselt Values	123

CONCLUSION	126
REFERENCES	127
CHAPTER 8 THEORETICAL STUDY OF THE GEOMETRICAL PARAMETERS EFFECT ON THE BEHAVIOR OF A SOLAR CHIMNEY POWER PLANT	129
<i>Haythem Nasraoui, Zied Driss and Hedi Kchaou</i>	
INTRODUCTION	129
MATHEMATICAL MODEL	132
Solution Process	138
RESULTS	140
Chimney Height Effect	140
Collector Radius Effect	141
Chimney Radius Effect	142
Collector Height Effect	142
CONCLUSION	143
REFERENCES	143
CHAPTER 9 NUMERICAL INVESTIGATIONS OF THE EFFECT OF PACKED BED POROSITY ON THE FLOW BEHAVIOR	146
<i>Hajer Troudi, Moncef Ghiss, Mohamed Ellejmi and Zoubeir Tourki</i>	
INTRODUCTION	146
METHOD	147
Packed Column Process	147
Governing Equations	148
Mesh and Boundary Conditions	149
RESULTS AND DISCUSSION	150
Effect of Grid Size	150
Model Validation by Experimental Data	150
Effect of Packed Porosity	151
CONCLUSION	154
REFERENCES	154
CHAPTER 10 COMPARISON BETWEEN A CONVENTIONAL AND A FOUR-STAGE SAVONIUS WIND ROTOR	156
<i>Sobhi Frikha, Zied Driss and Mohamed Salah Abid</i>	
INTRODUCTION	156
GEOMETRY SYSTEM	157
Savonius Wind Rotor	157
Wind Tunnel	159
NUMERICAL MODEL	159
NUMERICAL RESULTS	160
Velocity Field	161
Average Velocity	163
Static Pressure	164
Dynamic Pressure	165
Turbulent Kinetic Energy	166
Dissipation Rate of the Turbulent Kinetic Energy	167
Turbulent Viscosity	168
Vorticity	168
COMPARISON WITH EXPERIMENTAL RESULTS	169
Power Coefficient	169
Dynamic Torque Coefficient	170

CONCLUSION	171
REFERENCES	172
SUBJECT INDEX	174

PREFACE

This book focuses on the dissemination of information of permanent interest in mechanic applications and engineering technology. The considered applications are widely used in several industrial fields particularly in those of automotive and aerospace aspects. Many features related to Mechanic processes are presented. The presented case studies and development approaches aim to provide the readers, such as engineers and PhD students, with basic and applied studies broadly related to the Mechanic Applications and Engineering Technology.

In the first chapter, a numerical investigation of the turbulent forced convection of a water- Al_2O_3 nanofluid in slot jets impinging on multiple hot components fixed on the lower wall. The outcomes revealed that the increase in the Reynolds number and volume fraction of nanoparticles with all nanoparticle shapes enhanced the heat transfer rate.

The second chapter examines the experimental application of the gas scavenging membrane distillation (SGMD) process. This process was used to treat complicated solutions with volatile molecules to separate. The SGMD distillation unit has been modeled by mathematical equations and simulated to evaluate the effects of heat transfer and mass transfer.

The third chapter presents the integration of multilayer neural network with an expert system for the automatic choice of the design process of multi-spindle drilling housing. An intelligent design system approach was developed to integrate various phases of the mechanical process including neural network subclasses and MLANN.

The aim of the fourth chapter is to design a new hybrid solar collector based on the superposition of the thermal and electrical functions instead of their overlay as previously done in most existing systems. The main goals are to study the effectiveness of our PV/T prototype in terms of the produced thermal energy.

In the fifth chapter, a thermodynamic cycle simulation of a four-stroke spark-ignition engine was conducted to predict the engine performance. The single-zone model was built based on the Wiebe function for the mass fraction burned and Woschni's model for the convective heat loss. This study was performed to evaluate the effects of the combustion duration on the engine performance characteristics.

The sixth chapter focus on a Kerosene, Methane and Gasoil flame simulated with detailed chemistry. The mathematical model was based on the enthalpy conservation between two states, and this model was used with the first law of thermodynamics to define enthalpies of reaction and adiabatic flame temperatures at constant pressure.

In the seventh chapter, the laminar natural convection problem for a Newtonian fluid confined between two concentric ellipses was solved numerically. Two cases of heating were assumed, an inner wall at high temperature and an external one at low temperature, then the opposite. The effects of Rayleigh number, aspect ratio in addition to the ellipses orientations were investigated. The dynamic and thermal fields as well as the geometry average Nusselt number calculation were analyzed.

In the eighth chapter, a theoretical Solar Chimney Power Plant (SCPP) model was developed to study the impact of the main design parameters on the SCPP performance. Based on the Manzanares prototype, the proposed model was verified and validated with the experimental

ii

data. The thermodynamic characteristics of the SSCP were analyzed by varying the chimney height, the chimney radius and the collector radius.

The ninth chapter aims to develop a geometrical model of a packed column with one cone spray to simulate the injection. CFD simulations using the mixture model coupled with several turbulence models were used to analyze the porosity effect on the fluid profiles. The results confirmed that the decrease of the packed porosity resulted in a greater dispersion of the liquid, indicating the anisotropic behavior in the bed.

In the tenth chapter, the influence of the shape on the characteristics of a Savonius wind rotor was studied in numerical simulations and experimental measurements. Particularly, the features of the Savonius rotor with a new design rotor consisting of a four-stage configuration was studied. The experimental measurements were conducted in an open wind tunnel to validate the numerical model.

Zied Driss
Laboratory of Electromechanical Systems (LASEM)
National School of Engineers of Sfax (ENIS)
University of Sfax (US)
Sfax, Tunisia

List of Contributors

Ayoub Fajraoui	University of Tunis (UT), Engineering National High School of Tunis (ENSIT), Production and Energetics Laboratory (LMPE), Tunis, Tunisia
Aref Maalej	University of Sfax, National School of Engineers of Sfax, Laboratory of Electromechanical Systems (LASEM), 3038 Sfax, Tunisia Department of Electrical and Electronic Engineering Science, University of Johannesburg, Johannesburg, South Africa
Amara Ibraim	Higher Institute of Technological Studies of Nabeul, Mrezgua University Campus, Mrezga, Tunisia
Ali Damak	Laboratory of Electro-Mechanic Systems (LASEM), National School of Engineers of Sfax (ENIS), University of Sfax (US), 3038 Sfax, Tunisia
Abderrahmane Horimek	Department of Mechanical Engineering, Ziane Achour University, Djelfa, Algeria
Bouziane Boudraa	LEAP Laboratory, Department of Mechanical Engineering, University of Mentouri Brothers, Constantine, Algeria
Farhat Abdelmoumene	Department of Mechanical Engineering, Ziane Achour University, Djelfa, Algeria
Houssam Chouikhi	University of Sfax, National School of Engineers of Sfax, Laboratory of Electromechanical Systems (LASEM), 3038 Sfax, Tunisia Department of Mechanical Engineering, College of Engineering (CoE), King Faisal University (KFU), Hofuf, Al-Ahsa 31982, Kingdom of Saudi Arabia
Hatem Bentaher	University of Sfax, National School of Engineers of Sfax, Laboratory of Electromechanical Systems (LASEM), 3038 Sfax, Tunisia
Haythem Nasraoui	Laboratory of Electro-Mechanic Systems (LASEM), National School of Engineers of Sfax (ENIS), University of Sfax (US), 3038 Sfax, Tunisia
Hedi Kchao	Laboratory of Electro-Mechanic Systems (LASEM), National School of Engineers of Sfax (ENIS), University of Sfax (US), 3038 Sfax, Tunisia
Hajer Troudi	Laboratoire de Mécanique de Sousse (LMS), Ecole Nationale d'Ingénieurs de Sousse (ENISo), 4023 Sousse, Université de Sousse, Sousse, Tunisie
Kamel Mehdi	University of Tunis (UT), Engineering National High School of Tunis (ENSIT), Production and Energetics Laboratory (LMPE), Tunis, Tunisia
Mokhless Boukhriss	Higher Institute of Technology Studies of Kairouan, Kairouan, Tunisia Laboratory of Electromechanical Systems (LASEM), National Engineering School of Sfax, Sfax University, Sfax, Tunisia
Mohamed Ali Maatoug	Higher Institute of Technology Studies of Kairouan, Kairouan, Tunisia
Mahdi Timoumi	Higher Institute of Technology Studies of Kairouan, Kairouan, Tunisia
Mohamed Fterich	University of Sfax, National School of Engineers of Sfax, Laboratory of Electromechanical Systems (LASEM), 3038 Sfax, Tunisia
Mohamed Brayek	Laboratory of Electro-Mechanic Systems (LASEM), National School of Engineers of Sfax (ENIS), University of Sfax (US), 3038 Sfax, Tunisia

Mohamed Ali Jemni	Laboratory of Electro-Mechanic Systems (LASEM), National School of Engineers of Sfax (ENIS), University of Sfax (US), 3038 Sfax, Tunisia
Mohamed Salah Abid	Laboratory of Electro-Mechanic Systems (LASEM), National School of Engineers of Sfax (ENIS), University of Sfax (US), 3038 Sfax, Tunisia
Moncef Ghiss	Laboratoire de Mécanique de Sousse (LMS), Ecole Nationale d'Ingénieurs de Sousse (ENISo), 4023 Sousse, Université de Sousse, Sousse, Tunisie
Mohamed Ellejmi	Alpha Engineering International (AEI), Sousse, Tunisie
Nizar El Ouni	Higher Institute of Technology Studies of Kairouan, Kairouan, Tunisia
Nour Abdelkader	Laboratory of Dynamic of Engines and Vibroacoustics, University UMBB, Boumerdes, Algeria
Noureddine Ait-Messaoudene	Laboratoire des Applications énergétiques de l'Hydrogène (LApEH), University Blida 1, Blida, Algeria
Rachid Bessaïh	LEAP Laboratory, Department of Mechanical Engineering, University of Mentouri Brothers, Constantine, Algeria
Rachid Renane	Laboratory of Aeronautical Sciences, Institute of Aeronautics and Space Studies, University of Blida 1, BP 270 Roud of Soumaa, Blida, Algeria
Rachid Allouche	Laboratory of Aeronautical Sciences, Institute of Aeronautics and Space Studies, University of Blida 1, BP 270 Roud of Soumaa, Blida, Algeria
Sobhi Frikha	Laboratory of Electro-Mechanic Systems (LASEM), National Engineering School of Sfax (ENIS), University of Sfax, 3038 Sfax, Tunisia
Zied Driss	Laboratory of Electro-Mechanic Systems (LASEM), National School of Engineers of Sfax (ENIS), University of Sfax (US), 3038 Sfax, Tunisia
Zoubeir Tourki	Laboratoire de Mécanique de Sousse (LMS), Ecole Nationale d'Ingénieurs de Sousse (ENISo), 4023 Sousse, Université de Sousse, Sousse, Tunisie LMS ENISo-Université de Sousse, Directeur de la Mission Universitaire de Tunisie en Allemagne, Godesberger Allee 103, 53175 Bonn, Germany

CHAPTER 1

Numerical Investigation of Turbulent Slot Jets with Various Nanoparticles Shapes**Bouziane Boudraa^{1,*} and Rachid Bessaïh¹**¹ *LEAP Laboratory, Department of Mechanical Engineering, University of Mentouri Brothers, Constantine, Algeria*

Abstract: In this work, a numerical investigation related to the turbulent forced convection of a water-Al₂O₃ nanofluid in slot jets impinging on multiple hot components fixed on the lower wall, using different nanoparticle shapes (spherical, blades, bricks, cylindrical and platelets), was carried out. The standard k-ε turbulence model with wall enhanced treatment and two-phase mixture model were used to analyze the fluid flow and heat transfer. The outcomes revealed that the increase in the Reynolds number (Re) and volume fraction of nanoparticles (ϕ) with all nanoparticle shapes enhanced the heat transfer rate. The platelets nanoparticle's shape significantly contributes to increasing the heat transfer rate compared with other forms. Also, we have found that the two-phase mixture model gives a higher average Nusselt number (\overline{Nu}) values compared to the single-phase model, and the maximum values of \overline{Nu} is located around the last block due to the second jet's dominance (J2) compared to the first jet (J1). We have compared our results with those found in the literature.

Keywords: Forced convection, Nanoparticles shapes, Slot jets, Turbulence.

INTRODUCTION

Methods of improving heat transfer, such as jet impinging, are widely applied to achieve a higher heat transfer rate. Impinging jet is used in thermal processes such as textile products, food industry, cooling of microelectronic components, heat transfer of electronic parts, cooling of external walls of combustion engines, and cooling components of gas turbines [1, 2]. In the literature, several computational and experimental studies have been performed used the impinging jet in recent years [3 - 9], the same thing in the domain of nanofluids, many studies have been done [10, 11].

* **Corresponding author Bouziane Boudraa:** LEAP Laboratory, Department of Mechanical Engineering, University of Mentouri Brothers, Constantine, Algeria; E-mail: bouziane.boudraa@umc.edu.dz

Most of the numerical analysis studies have been performed utilizing the single-phase method. Safaei *et al.* [12] experimentally performed a thermal analysis of the base fluid in the pool boiling system of glycol - water alumina nano-suspension. Giwa *et al.* [13] examined the influence of base fluid, temperature and ϕ on the thermophysical properties of hybrid nanofluids alumina-ferrofluids ($\text{Al}_2\text{O}_3\text{-Fe}_2\text{O}_3$). Lee *et al.* [14] examined the effect of a confined air jet experimentally. They discovered that the maximum heat transfer rates are found at the point of stagnation. Lafouraki *et al.* [15] used a numerical simulation to investigate the heat transfer on a confined jet. Results showed that an increase in ϕ leads to a rise in \overline{Nu} , as the skin friction coefficient (\overline{Cf}) decreases with an increase in Re and the ratio between the channel height and the nozzle of the diameter. Abdelrehim *et al.* [16] studied the single-phase model and two-phase mixture model of nanofluid on heat transfer properties, and then the models were compared with each other. Results reveal that two-phase mixture model gives higher values of \overline{Nu} . The effect of several parameters, such as Re and ϕ , has been analyzed numerically by Selimefendigil and Öztop [17]. Data obtained by researchers indicate that with rising Re and ϕ , the heat transfer boosts. Selimefendigil and Öztop [18] conducted a numerical analysis using nanofluids to cool an isothermal hot surface with an adiabatic rotating cylinder. It was discovered that the (\overline{Nu}) was enhanced with Re ; in addition, the heat transfer rate is higher when the cylinder was closest to the jet inlet. A numerical simulation in a confined jet using water- Al_2O_3 nanofluid was performed by Rahimi-Esbo *et al.* [19]. Results show that raising the values of Re , ϕ and the ratio between the channel height and the nozzle length leads to an increase in the values of \overline{Nu} . Lavouraki *et al.* [20] conducted a numerical study of a confined jet using two-phase mixture model. The outcomes indicate that \overline{Cf} and \overline{Nu} decrease and increase, respectively, with a higher of Re , ϕ and ratio between the channel height and the nozzle length. To study the influence of uniform and non-uniform speed of impact jets, a numerical study is carried out by Izadi *et al.* [21] The results indicate that raising the values of ϕ enhances the heat transfer rate. Additionally, when using a non-uniform impingement jet with a low-speed distribution, the thermal performance is improved. Lamraoui *et al.* [22] investigated numerically the flow characteristics in a confined jet by considering the nanofluid as Newtonian and non-Newtonian. It was found that \overline{Nu} is much higher for non-Newtonian nanofluid than Newtonian flow. Paulraj and Sahu [23] performed numerical research on the flow and heat transfer of the laminar impinging jet using a two-phase mixture model at different types of nanofluids. They observed that the heat transfer rate rises with a decline in the size of nanoparticles. In addition, they discovered that the Al_2O_3 -water nanofluid produced the highest values of Nusselt number relative to other nanofluids. Oil/MWCNT nanofluid flow within a two-dimensional microchannel with nanofluid jet injection placed on the lower surface was

examined by Jalali *et al.* [24]. The findings show that the values of \overline{Nu} dramatically rising with the increase in the number of fluid jets, ϕ and Re . Researchers in this analysis also have observed that by applying the slip boundary condition on solid walls the crossed fluid momentum increases considerably. The influence of bed roughness on properties of turbulent confined wall jets has been experimentally studied by Shojaeizadeh *et al.* [25]. It was observed that by changing the surface roughness, the highest value of the turbulence strength is raised. Bagherzadeh *et al.* [26] performed a computational analysis on the flow and heat transfer of the two-dimensional microchannel with numerous impinging jets utilizing slip boundary with a homogeneous magnetic field using Water/ Al_2O_3 nanofluid. Data indicated that a rise in intensity of the magnetic field, Re and ϕ leads to an enhancement of \overline{Nu} . The impact of thermal boundary conditions on the heat transfer activity of a laminar confined slot jet affecting walls of various geometries (flat, convex, and concave) was experimentally analyzed by Han *et al.* [27]. Researchers discovered that in the wall jet zone, the uniform heat flux conditions dramatically enhance \overline{Nu} in comparison to the uniform wall temperature. The cooling efficiency of the impinging synthetic jet using various nanofluids was analyzed numerically by Lau *et al.* [28]. Researchers have observed that the total thermal efficiency is greatly affected by nanofluids' thermal conductivity and dynamic viscosity. To minimize the temperature of electronic systems, Zunaid *et al.* [29] studied the thermal efficiency of a set of inclined microjets. Researchers confirmed that the average temperature of the surface is reduced as the number of impingements rises. Pal *et al.* [30] studied the interaction between two impinging fluid jets in a closed impinging jet reactor. Shi *et al.* [31] have experimentally examined the influence of nano-alumina additives on the instability of circular jets at low speed. A numerical analysis of various configurations was developed when applying Al_2O_3 nanofluid to a highly Reynolds turbulent jet by Granados-Ortiz [32]. The computational study revealed that with all the simulations done, the application of nanoparticles boosts the heat transfer. Shirvani *et al.* [33] Numerically evaluated the influence of the forms of nanoparticles on the heat transfer and flow characteristics of impingement jets. The results indicate that the highest \overline{Nu} leads to a maximum heat transfer related to nanofluids with platelet and cylindrical nanoparticles. In contrast, the lowest heat transfer rate is associated with fluids containing spherical nanoparticles. Al_2O_3 water nanofluid was numerically tested for various nanoparticle forms on flat and triangular-corrugated impinging surfaces by Ekiciler *et al.* [34]. The analysis findings indicate that the nanoparticle form of the platelet displays the maximum heat transfer rate. Amjadian *et al.* [35] experimentally studied the properties of the impact jet on a hot surface using CuO-water nanofluid. Results showed that the rise in Re and ϕ increases the heat transfer coefficient. The heat transfer properties of air/nanofluid jet cooling flux on a rotating hot circular disk, using a multiphase

CHAPTER 2

The Experimental Study on a Sweeping Gas Membrane Distillation Unit**Mokhless Boukhriss^{1,2,*}, Mohamed Ali Maatoug¹, Mahdi Timoumi¹ and Nizar El Ouni¹**¹ Higher Institute of Technology Studies of Kairouan, Kairouan, Tunisia² Laboratory of Electromechanical Systems (LASEM), National Engineering School of Sfax, Sfax University, Sfax, Tunisia

Abstract: This document examines the experimental application of the gas scavenging membrane distillation (SGMD) process and its advantages and disadvantages. SGMD is the least used configuration in membrane distillation (MD), and it is more expensive to build. Scavenging Gas Membrane Distillation (SGMD) is used to treat complicated solutions with volatile molecules to separate. In this study, heat and mass transport mechanisms, as well as modeling and simulation studies, are systematically reviewed. In SGMD, the main operating parameters are supply temperature, supply flow rate, gas temperature, and gas flow rate. Furthermore, the performance of SGMD is discussed and highlighted. Potential applications and areas in which SGMD could excel are mentioned. Finally, future research opportunities in SGMD are identified.

A hollow fiber scavenging gas membrane distillation (SGMD) module is examined in this study. Our SGMD distillation unit has been modeled by mathematical equations and simulated by a runtime program on Matlab software to evaluate the effects of heat transfer and mass transfer. Also, we have found that the heat and mass transfer in our SGMD desalination system is defined by the temperature evolution in the vaporization chamber and the inert gas velocity of the gas. The model predicts a small error of 3.6% with the experimental data reported in the literature, indicating the reliability of simulated results.

Keywords: Collector Solar, Desalination, Energy, Fluid Velocity, SGMD.

INTRODUCTION

Nowadays, the increase in the world population leads to an increase in the consumption of drinking water by individuals, followed by agrifood and the production of manufactured goods.

* **Corresponding author Mokhless Boukhriss:** Higher Institute of Technology Studies of Kairouan, Kairouan, Tunisia and Laboratory of Electromechanical Systems (LASEM), National Engineering School of Sfax, Sfax University, Sfax, Tunisia; E-mail: mokhlessiset@yahoo.fr

The main desalination processes for freshwater production include Reverse osmosis (RO), multi-stage flash distillation (MSF), multiple-effect distillation (MED), and membrane distillation.

The MD process has four configurations which are: Direct Contact Membrane Distillation (DCMD), Air Gap Membrane Distillation (AGMD), Sweep Gas Membrane Distillation (SGMD), and Vacuum Membrane Distillation (VMD). These possibilities have their advantages and disadvantages. Several research works have been conducted on DCMD. However, limited data are available on SGMD [1, 2]. SGMD configuration leads to low conductive heat loss with reduced resistance to mass transfer and good future prospects.

In this work, we present an experimental study on the SGMD configuration. Our model is based on the effects of temperature on heat and mass transfer mechanisms and temperature profiles in the two system chambers. The experiments mainly examine the role of relevant parameters, such as the inlet and outlet temperatures and the circulation speeds of the two fluids. The experimental results have been discussed on the basis of the model, which are in good agreement with the previous findings. The model developed in the SGMD process is based on the phenomena of mass and heat transfer in this type of technology [3, 4]. The experimental results are studied on a pilot plant of the PTFE type (500 l) represented by Fig. (1a and b) [5, 6].

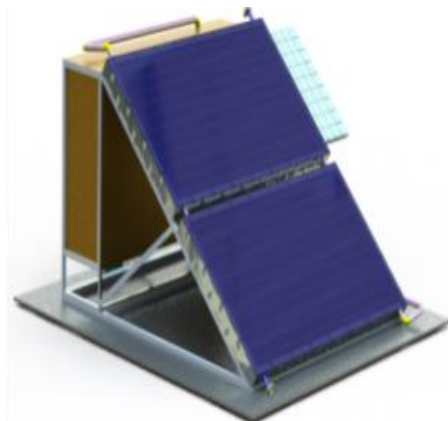


Fig. (1a). SGMD desalination unit.

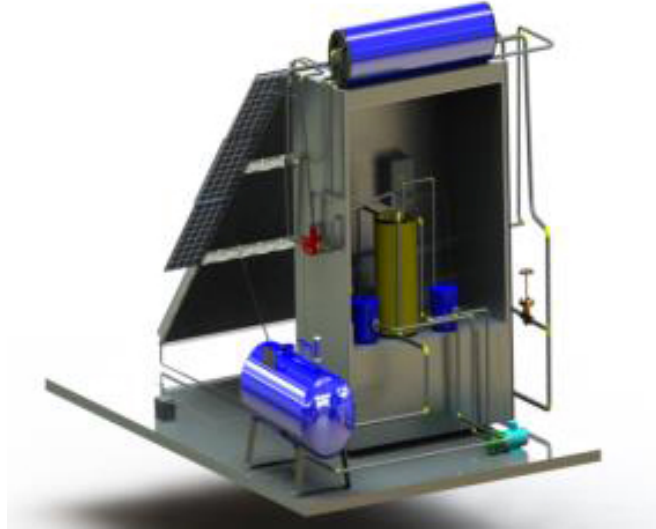


Fig. (1b). SGMD desalination unit.

THEORETICAL MODEL STUDY

There are two theoretical approaches used to calculate the heat and mass transfer, and thus calculate the temperatures in the evaporation and condensation chambers, the concentrations, and the permeate fluxes in the SGMD module. In the experimental study, the hot water circulates in the evaporation chamber, and the inert gas passes in the condensation chamber membrane.

There are three types of variables [9, 10]:

1. The input variables, $u(t)$, which are temperature, gas storage and affect the correct functioning of the processes.
2. The output variables, $y(t)$, are process variables controlled by a predefined set point or range.
3. These internal variables, $z(t)$, are necessary to solve the mathematical model equations of the SGMD system. These variables are linked to the inputs of the SGMD system components. Template input parameters are mentioned in Fig. (2), and the variables are defined in Table 1.

Development of Design Processes for Multi-Spindle Drilling using the Neural Network and Expert System

Ayoub Fajraoui^{1*} and Kamel Mehdi¹

¹ University of Tunis (UT), Engineering National High School of Tunis (ENSIT), Production and Energetics Laboratory (LMPE), Tunis, Tunisia

Abstract: This work presents the integration of multilayer neural network with an expert system for the automatic choice of the design process of multi-spindle drilling housing. An intelligent design system approach is developed to integrate various phases of the mechanical process including neural network subclasses and MLANN. This solution reduces the time during the design preparation process and to improve production. The automatic choice is carried out in three steps: Firstly, we started with the formulation of training base experiments of the experts of the field as well as the necessary knowledge of expertise, and which is among the general criteria for the choice of the design process. The second step was devoted to the creation of many multi layers NN1...NNm for the choice of the design mode. The final step is related to the application of the outputs as results and an input for chaining by the expert system. This chaining is based on several models based chaining (input data collection) from the neural network results and processing (output results). The results are the kinematics schema of the multi spindle drilling housing.

Keywords: Computer Aided Design, Design Methodology, Expert System, Mechanical Design, Neural Networks, Object-Oriented Language.

INTRODUCTION

The design process of the mechanical products is tedious and time consuming because of the various stages and complex activities involved. On the other hand, there is a strong pressure to reduce the overall costs in a competitive market environment [1]. However, the traditional design approach is inadequate in meeting these needs. Today a lot of mechanical design application software and different databases were used for mechanical design studies, but these technologies were distributed and there was no coordination between these.

* Corresponding author Ayoub Fajraoui: University of Tunis (UT), Engineering National High School of Tunis (ENSIT), Production and Energetics Laboratory (LMPE), Tunis, Tunisia; E-mail: ayoub.fajraoui@gmail.com

Therefore, a number of researchers have focused their studies on establishing a cooperative and integrated environment. Su and Wakelam [2] studied an intelligent hybrid system for integration in design and manufacturing. Their approach combines a rule based system, artificial neural networks, genetic algorithm, and hypermedia and CAD package into a single environment. The expert system is capable of computational, qualitative, descriptive and explanatory functions. An additional advantage of the expert system is its ease of use, in a process which boils down to a series of questions and answers between the computer program and the user, in which the system receives relevant information, not only from the user but also from external sources of knowledge, such as spread-sheets, and other calculation tools [3].

LITERATURE REVIEW

Several research studies show the effectiveness of neural networks and expert system to be complex modeled nonlinear behaviors. Several research studies show the effectiveness of neural networks and expert system to be complex modeled nonlinear behaviors. The examples include a work by Kuo and Wu [4], which covers the prediction of the sheet thinning in a hydrodynamic forming process. Xiong and Withers [5] also investigated a recurrent neural network model for the prediction of the damage evolution during hot non uniform, non-isothermal forging on the basis of a limited number of damage snapshots during the process. In 2005, Sanjay *et al.* [6] modeled a tool wear in drilling by statistical analysis and artificial neural network.

The first works using artificial neural networks in mechanics, began in the field of robotics. The use of the neural networks emerged in the 1980s because of their ability to approach multidimensional functions from a small number of learning samples. Many Network architectures have been studied for robot control, with various control approaches, the role of networks and learning [7]. The first article in the field of structural mechanics was published by Adeli and Yeh in 1989 [8]. Since then, RNA applications in mechanics have progressed quickly. They are used as a tool for classification, modeling and identification.

For the expert systems, a number of researchers have worked in the area of parameters selection for a sustainable product design. Holloway, Skerlos *et al.* [9] developed a new method of material selection in mechanical design: the material selection charted off by Ashby showed how this methodology can be extended to consider environmental factors. Ermolaeva *et. al* [10] took the example of the application of a structural optimization system to the optimal choice of foams for the use as floor panels in the bottom structure of a car. In addition to the optimal (minimized) mass and materials price used for the selection of foams, the

assessment of an environmental impact of candidate materials during the entire life cycle of the structure was considered. Giudice *et al.* [11] proposed a selection procedure that elaborates data on the conventional and environmental properties of materials and processes and calculates the values assumed by functions, which quantify the environmental impact over the whole life cycle and the cost resulting from the choice of materials. Chan and Tong [12] proposed a gray relational analysis for aggregating multiple and contradictory objectives of sustainable material selection. Rafiee *et al.* [13] have developed a new procedure that recognizes experimentally gear defects of a typical transmission system using a multilayer perceptron neural network. Kong *et al.* [14] performed experiments to identify the isomorphism of the mechanism kinematic chain. The adopted model is a drilling housing with one input and 4 outputs (4 pins). According to Turban *et al.* [15] and Van Ekris *et al.* [16], both advisory and expert systems are problem solving packages that mimic a human expert in a special area. These systems are constructed by eliciting knowledge from human experts and coding it into a form that can be used by a computer in the evaluation of alternative solutions to problems within that domain of expertise. On the other hand, Gregg and Walesa [17] stated that advisory systems are designed to support decision making in more unstructured situations, which have no single correct answer.

DESIGN METHODOLOGY

The entry level has neurons that represent the network input units and adapt the sample for the network processing. At the hidden level, the nodes represent the hidden network units and ensure the nonlinearity network. The output level contains the output neurons that have the possible codes values and joins them in the sample after analysis. In front of its biological counterpart, the artificial neural network is not able to react to an unknown problem. The neural network must be “trained”. The network formation is based on a number of known relationships between the input and output values. The neural network is fully formed when the response of the input sample is within the expected output acceptable error tolerance.

Application of Artificial Neural Networks

For technical and scientific reasons, neural networks are used in the minds of engineers and decision makers including modeling and process control. The Neuronal approach has become a need in very diverse areas of industry and services. The artificial neural network approach is used mainly in complex problems that are not solved by linear systems. The idea of using artificial neural networks started with biological neurons. In this context, new techniques should be sought for the automatic generation of gearboxes design mainly based on

CHAPTER 4

Experimental Investigation of a New Hybrid Solar Collector (PV/T) System

Mohamed Fterich^{1,*}, Houssam Chouikhi^{1,2}, Hatem Bentaher¹ and Aref Maalej^{1,3}

¹ University of Sfax, National School of Engineers of Sfax, Laboratory of Electromechanical Systems (LASEM), 3038 Sfax, Tunisia

² Department of Mechanical Engineering, College of Engineering (CoE), King Faisal University (KFU), Hofuf, Al-Ahsa 31982, Kingdom of Saudi Arabia

³ Department of Electrical and Electronic Engineering Science, University of Johannesburg, Johannesburg, South Africa

Abstract: Solar Energy can be exploited to produce heat and/or electricity. PV/T panels are a good application to produce both photovoltaic and Thermal energies by recovering heat lost with a heat removal fluid (water or air). This induces an improvement of the energetic efficiency of the panel since it is the addition of electrical and thermal outputs. The object of this work was to design a new hybrid solar collector based on the superposition of the thermal and electrical functions instead of their overlay as previously done in most existing systems. Indeed, while thermal energy production requires high fluid operating temperatures, PV electrical energy production needs relatively low operating temperatures. The main goals are to study the effectiveness of our PV/T prototype in terms of thermal energy produced. Moreover, the present system improves the promotion of agro-food micro-enterprises by the integration of miniaturized machines with dryers in remote areas where electric connectivity is not available. In these sites, the farmers can dry the various agricultural products using the prototype we have realized.

However, we dealt with an experimental analysis to study the influence of external and internal parameters on the thermal and electrical performance of a photovoltaic thermal hybrid collector PV/T. The system consists of a photovoltaic-thermal (PV/T) air collector of 1.37 m². A fan was used to force the convection. Based on the experimental results, it was observed that the thermal and electrical energy was increased when mass flow rate and solar radiation were increased. The thermal and electrical efficiency generated by the system was calculated as 65% and 12.5%, respectively. It was also observed that the outlet air temperature increased.

* **Corresponding author Mohamed Fterich:** University of Sfax, National School of Engineers of Sfax, Laboratory of Electromechanical Systems (LASEM), 3038 Sfax, Tunisia;
E-mail: mohamedfterich@gmail.com

Keywords: Experimental Investigation, Photovoltaic-thermal collector, Renewable Energy, Solar Energy, Thermal Efficiency and Electrical Efficiency.

INTRODUCTION

The energy needs of the whole world are on the continuous rise and among the alternative sources of renewable energy, solar energy is currently experiencing great development. One of the developed ways in solar energy exploitation is the use of hybrid solar panels, which produce electricity and heat at the same time [1]. The PV/T solar collector is one of the devices used in solar energy. Therefore, many studies on the PV/T collectors have been extensively used theoretically and experimentally [2]. Many PV/T collectors' designs have been developed and can be divided into several categories, either according to the nature of the fluid used (air or water) or the presence of an additional glass cover (covered and non-covered collectors). Compared with the solar thermal collectors or the PV modules, the market for the PV/T modules is still very small today, but the interest in this technology has been increasing in the past decade [3]. Various kinds of PV/T collectors/systems were proposed in the past. The solar collector photovoltaic/thermal hybrid (PV/T) converts the solar energy into heat and electricity. In other words, the PV is used as a thermal absorber [4]. The advantages of combining a thermal collector and a photovoltaic panel in only one collector are the increase of the total efficiency of the solar energy conversion and the architectural uniformity in the case of use. The hybrid solar collectors allow reducing the operating temperature of the photovoltaic panels and therefore improving their electrical efficiency by recovering the energy that dissipates in the form of heat and thus increasing their outputs [5]. The PV/T collectors have recently been utilized in different industries, which motivated researchers in different fields of study to perform and develop experimental and numerical methods [6]. He *et al.* designed a PV/T collector adopting an aluminum-alloy flat-box as the absorber, and test results showed that the daily thermal efficiency of this collector was found around 40% [7]. Zondag *et al.* listed different designs for PV/T collectors in their paper, and deemed that the sheet and tube design was one of the best designs because it was easier to manufacture [8]. Various authors from time to time have used different methods to reduce the PV cell temperature to improve the electrical efficiency of the PV cell and the thermal performance of the PV/T. The pattern of airflow inside the photovoltaic thermal air collector (PV/T) is a dominating factor, as reported by Hegazy *et al.* It has been found that thermal efficiency has enhanced when the flow of air took place above the heated plate [9]. In work reported by Charalambous *et al.* [10], the airflow below the heated plate resulted in a better gain of energy. The effect of the single-pass and the double pass airflow has been investigated by Slimani *et al.* [11] where it was reported that the double pass PV/T has the overall thermal efficiency of best as

compared to single-pass PV/T. This research is in line with the study conducted by Sopian *et al.* [12]. where the double pass airflow has the highest overall efficiency due to better heat extraction against single-pass airflow. Tiwari *et al.* [13], carried out an analytical study for the prediction of water temperature of an integrated photovoltaic thermal solar (PV/T) water heater under constant mass flow rate. They carried out the analysis using basic energy balance for hybrid collector (PV/T) and storage tank, in terms of design and climatic parameters, respectively. It is observed that the overall daily thermal efficiency of the PV/T system increases with the increases of the constant mass flow rate of the circulating fluid, but collection temperature decreases. Tonui and Tripanagnostopoulos [14] improved the PV/T air collectors by enhancing heat extraction. They addressed some inherent shortcomings of the PV/T air collectors, such as the low density, volumetric heat capacity and air thermal conductivity using a thin suspended flat metallic sheet between the absorber surface and back plate and/or using fins on the air duct back plate. They report energy efficiencies of 30%, 28% and 25%, respectively, for finned, suspended metallic plates and normal air heaters. The choice of a particular design depends on location, especially latitude. The use of finned systems is advantageous for higher latitudes where higher heat gains are needed in winter, whereas the PV/T system with a suspended metallic sheet is usually preferable for low latitude or tropical countries. Dubey *et al.* [15] developed an expression for the PV/T air collectors electrical and thermal efficiencies as a function of climatic and design parameters, and applied it to several cases. Thermal Energy can then be used for many applications like solar heating, space heating, *etc.* However, hybrid solar collectors (PV/T) that provide both electricity and heat are increasingly becoming more popular in the world [16]. Even so, further strategies are required to cool the PV module, to improve the electrical performance [17]. Furthermore, these devices allow the opportunity to exploit the heat in the module in other applications such as drying purposes of agro-food products [18]. Agriculture crop drying has advanced notably in decades in terms of efficiency and reliability due to the solar collector [19].

In the present study, a non-destructive modification was performed on a conventional photovoltaic panel incorporating an air heat exchanger behind the PV recovering waste heat. The PV/T was directed to the south with an angle of 45 degrees horizontally to receive maximum radiation. The air flux enters the aluminum tubular canals located under the PV panel and spreads simultaneously into an upper gap. Consequently, it provides heat exchange in both faces of the panel PV, which helps to cool the photovoltaic cells and to carry the thermal energy to the drying room. The objective of our study was to minimize the operating temperature of the photovoltaic module by taking a maximum of heat and then using it to heat the air for drying. To this end, we developed and

Theoretical Study of the Effects of Combustion Duration on Engine Performance

Mohamed Brayek^{1,*}, Amara Ibrahim², Mohamed Ali Jemni¹, Ali Damak¹, Zied Driss¹ and Mohamed Salah Abid¹

¹ Laboratory of Electro-Mechanic Systems (LASEM), National School of Engineers of Sfax (ENIS), University of Sfax (US), 3038 Sfax, Tunisia

² Higher Institute of Technological Studies of Nabeul, Mrezgua University Campus, Mrezga, Tunisia

Abstract: In this study, a thermodynamic cycle simulation of a four-stroke spark-ignition engine was conducted to predict the engine performance. The single-zone model was built based on the Wiebe function for the mass fraction burned and Woschni's model for the convective heat loss. The first law of thermodynamics was applied to describe the engine behavior *versus* the crank angle. These formulas determine in-cylinder pressure, temperature, mean effective pressure, and effective power. This study was performed to evaluate the effects of the combustion duration on the engine performance characteristics. Simulations were carried out on a 98 cm³ four-stroke SI engine set up at 3600 rpm corresponding to the maximum torque (5.7 Nm).

In this study, it was found that under the same operating conditions, accelerating the combustion does not always increase the power delivered by the engine. The best engine performance in terms of compromise between heat losses and power delivered was obtained for the combustion duration corresponding to 60° CA.

Keywords: Combustion Duration, Combustion Modeling, Matlab, Performance Characteristics, Simulation, Spark Ignition Engine.

INTRODUCTION

The combustion duration is one of the most critical and important parameters affecting engine performance. The investigation of the effects of this parameter on the combustion cycle should be conducted in both ways, experimentally and analytically. Some recently published research has studied experimentally the parameters affecting combustion duration, such as fuels, engine speeds, ignition timing and engine load conditions.

* Corresponding author **Mohamed Brayek:** Laboratory of Electro-Mechanic Systems (LASEM), National School of Engineers of Sfax (ENIS), University of Sfax (US), 3038 Sfax, Tunisia; E-mail: medbrayek@gmail.com

Sun *et al.* studied the trend of combustion duration in HICE. Results show that, when using the lean mixture, the increase of engine speed reduces the combustion duration sharply. However, the combustion duration is practically independent of engine speed when the equivalence ratio is higher than 0.6 [1].

In their experimental research, Dhole *et al.* investigated the effects of the use of hydrogen as a dual fuel on the combustion duration and ignition delay of a dual fuel diesel engine. Results showed that at lower load with the addition of 30% of hydrogen as secondary fuel, the combustion duration increased by 2.5 degrees CA and ignition advance decreased by 2 degrees CA.

At 80% load and 50% volume of hydrogen in the fuel, the maximum increase in the combustion duration and decrease in the ignition advance were 9 and 6 degrees CA, respectively.

Furthermore, it was found that not only the type of gaseous fuels and their concentrations affect the combustion duration and ignition delay of the dual-fuel engine, but there are other parameters such as pressure, temperature, and oxygen concentration [2].

Chunhua *et al.* studied the effect of combustion duration on NO_x emission using a dual-fuel diesel-LNG engine. They concluded that the NO_x emission increases when the combustion duration increases before the top dead center (TDC). At a low engine load condition, an increase in combustion duration after the top dead center of CA reduced the Nox by 16.7%, but THC and CO emissions increased [3].

Lata *et al.* experimentally investigated the effect of using hydrogen and LPG as secondary fuels on the performance of a 4 cylinder (turbocharged and intercooled) genset dual-fuel diesel engine. It was found that peak cylinder pressure and combustion duration increased by 8.44 bar and 5 deg CA, respectively, when 30% of hydrogen was used alone as secondary fuel. When the same percentage of LPG was used, the peak cylinder pressure and combustion duration were found to be 6.95 bar and 5 deg CA, respectively. One important finding was that a significant enhancement in engine performance was obtained when a mixture of hydrogen-LPG was used as the secondary fuel [4].

In order to reduce the period of the experimental operations, the development relevant to the internal combustion engine is astonishing. Developing new models allows researchers and scholars to enhance the engine performance characteristics. Several parameters are crucial in the design and improvement of the engine characteristics. The challenge in engine modeling is to describe an engine by establishing relationships between the main engine input and output variables that

best describe the model and predict the engine performance in the different working conditions.

Hakan and Orhan studied the effect of air-fuel ratio, engine speed, spark advance, and compression ratio on the combustion duration. They developed an empirical correlation to determine combustion duration [5].

Several researchers have presented rigorous works in the field to develop thermodynamical models in order to describe the relationship between input parameters and the engine outputs. The input variables in the engine modeling are usually the engine geometries (bore, stroke, compression ratio, *etc.*), the engine speed, the spark advance angle, the combustion duration and the fuel characteristics (mass and heating values). The output variables are pressure, temperature, heat loss and cumulative work.

Chaudhari *et al.* implemented a single-zone, zero-dimensional model for any hydrocarbon fuel in Simulink to test the performance of a spark-ignition engine. The simulation results showed that the peak pressure during combustion dropped with a decrease in intake pressure which was similar to the experimental trend [6].

Shingne *et al.* implemented a combustion model for compression ignition combustion in GT-Power. Their analysis revealed that ignition timing is primarily a function of the charge temperature, and that the combustion duration is largely a function of ignition timing [7].

Al-Baghdadi developed a mathematical and simulation model to simulate a 4-stroke cycle of a spark-ignition engine fueled with hydrocarbon, hydrogen and ethanol singly or in a blend. The simulation results showed that adding hydrogen reduced the ignition delay, improved the combustion process, especially in the later combustion period, sped up the flame front propagation and reduced the combustion duration [8].

Caton studied the maximum temperature of the cylinder with respect to the fuel-air ratio, compression ratio and spark timing using a three-zone model for the combustion process [9]. He developed a thermodynamic simulation for the SI engine cycle. Results obtained with a single zone model were compared with those obtained from the multiple zone simulation. He showed that a multiple-zone model provides an additional insight into the major processes relative to the use of a single zone approach.

Eriksson and Andersson developed an analytical model used for cylinder pressure in spark-ignited engines based on the parameterization of an ideal Otto cycle and a set of tuning parameters [10]. Experimental validation using two engines

Effects of Preheating Temperature and Fuel-Air Equivalence Ratio on Pollution Control in Hydro Carbon Combustion

Rachid Renane^{1,*}, Rachid Allouche¹ and Nour Abdelkader²

¹ Laboratory of Aeronautical Sciences, Institute of Aeronautics and Space Studies, University of Blida 1, BP 270 Roud of Soumaa, Blida, Algeria

² Laboratory of Dynamic of Engines and Vibroacoustics, University UMBB, Boumerdes, Algeria

Abstract: Burning fossil fuels produces a great part of our energy production today and probably it will still do for at least the next few decades. Combustion is encountered in many practical systems such as heaters, power plants, aeronautic engines, buildings, *etc.* The growing expectations on increasing efficiency and reducing fuel consumption and pollutant emissions make the design of combustion systems much more complex and the science of combustion a rapidly expanding field. Comprehension and analysis of complex physical mechanisms start with the study and control of temperature and species in flame is an important challenge for industrial and environmental issues. We focus our study on a Kerosene, Methane and Gasoil flame simulated with detailed chemistry. The mathematical model is based on the enthalpy conservation between two states, and this model is used with the first law of thermodynamics to define enthalpies of reaction and adiabatic flame temperatures at constant pressure [1, 4]. To reach this objective, we must know the products of complete hydrocarbon combustion and all species of combustion products after dissociation and their molar fractions and equilibrium equations of dissociation reactions. Also, we calculate the elementary equilibrium reactions enthalpy and entropy by using (Bonni Mc Bride *et al.*) coefficients [2, 3] to compute thermodynamic functions such as specific heat, enthalpy and molar entropy. The obtained system of equations is resolved by Newton Raphson method. Among the obtained results are: To reduce the pollutants (CO₂, CO) and the fuel consumption, the mixture of fuel-air must be lean, therefore, the equivalence ratio must be lower than the unit. According to this study, if the fuel consumption is reduced *via* the equivalence ratio from 1.1 to 0.95, the combustion temperature remains constant, however, the production of CO will be reduced by 25%.

Keywords: Adiabatic flame temperature, Combustion, Fuel-Air equivalence ratio, Hydrocarbon, Pollution, Preheating.

* Corresponding author Rachid Renane: ILaboratory of Aeronautical Sciences, Institute of Aeronautics and Space Studies, University of Blida 1, BP 270 Roud of Soumaa, Blida, Algeria; E-mail: r.renane@gmail.com

INTRODUCTION

The requirements in energy are insured at present for the most significant part by the active combustion of hydrocarbons. Human activities like using the fossil fuels have a growing influence on the climate conditions and the pollution rate [5]. These activities lead to the release of huge amounts of greenhouse gases, which add to those naturally present in the atmosphere, thus reinforcing the greenhouse effect and global warming. CO₂ is the most produced greenhouse gas by human activities; its concentration in the atmosphere is currently higher than that at the beginning of industrialization [9 - 12]. To fight against pollution and global warming, which has a disastrous effect on human life, it is obvious and necessary to reduce emissions of gaseous pollutants. For this, the chemical potential stored in natural fuels is converted into thermal energy then to mechanical energy in the traditional installations (power stations, turbojets, gas turbines, automobiles, *etc.*). The knowledge of the thermodynamic properties of combustion products and the determination of their state immediately after the chemical reaction at the end of given evolutions are of crucial importance in the study of the thermal machines and subsequently reducing fuel consumption and pollutants emissions [22]. Several studies have been done in this context, we can cite the study which focuses on how human activity influences the air quality and measures that can be taken to reduce air pollution [5 - 8]; also, the contribution which calculates the behavior of methane combustion parameters for various initial temperatures [27, 29], another study demonstrates the contribution of dissociation product on the behavior of the adiabatic flame temperature of a hydrocarbon/air mixture as a function of the fuel concentration [28]; we can also cite the study which treats the effect of the initial temperature on the structure of laminar CH₄/air premixed flames. This clearly shows that the quantity of heat released from the combustion of methane is proportional to the imposed initial temperature [30]. Our contribution is a numerical study that exposes the influence of temperature variation of unburned gases on the structure of the flame front temperature, as well as the effect of Fuel-Air equivalence ratio on the combustion products and pollutants formation that allows us to deduce which parameters ensure higher efficiency with less fuel consumption and fewer pollutants (Fig. 1).

ASSUMPTIONS ON THE MODE OF COMBUSTION

To describe the state of the studied reactive flow, it is useful to introduce the following assumptions [13 - 15]:

- a. In this study, the combustion is adiabatic, isobar and it can be premixed or not premixed,
- b. The flame is considered laminar and stationary,

- c. The flow Mach number is low so that the kinetic energy and viscous dissipation can be neglected.

The assumption (a) depends on the way adopted to introduce the reactants into the combustion zone and this is one of the main parameters controlling the flame regime. Fuel and oxidizer may be mixed before the reaction occurs (premixed flame, Fig. 2), or enter separately in the reaction zone (non-premixed or diffusion flame, Fig. 3).

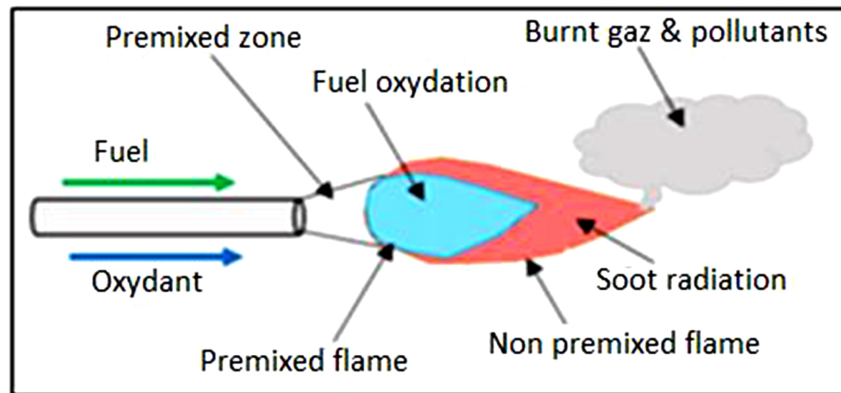


Fig. (1). Combustion process and production of pollutants.

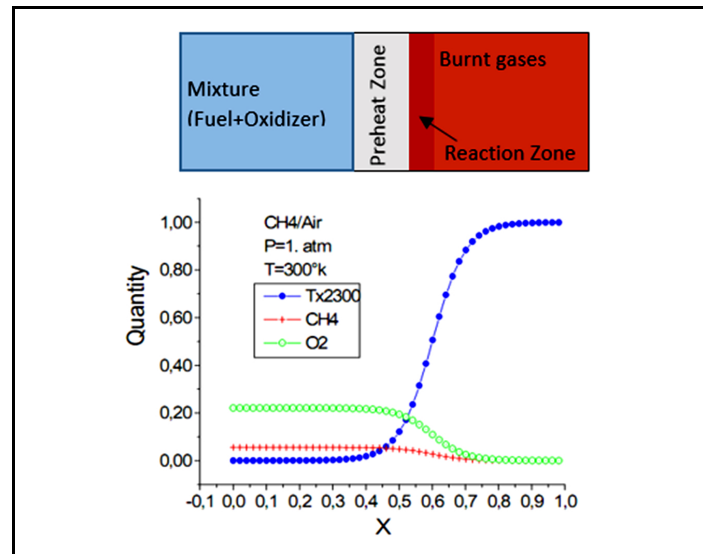


Fig. (2). Structure of premixed laminar flame.

CHAPTER 7

Numerical Study of Natural Convection between Two Concentric Ellipses with Different Shapes and Imposed Temperatures

Abderrahmane Horimek^{1,*}, Farhat Abdelmoumene¹ and Nouredine Ait-Messaoudene²

¹ Department of Mechanical Engineering, Ziane Achour University, Djelfa, Algeria

² Laboratoire des Applications énergétiques de l'Hydrogène (LApEH), University Blida 1, Blida, Algeria

Abstract: In this work, the laminar natural convection problem for a Newtonian fluid confined between two concentric ellipses is solved numerically. Two cases of heating are assumed, an inner wall at high temperature (T_H) and an external one at low temperature (T_C), then the opposite. Starting from the case of two circles (ellipses with equal diameters) and arriving at two ellipses, 25 geometries are studied for each type of heating, which gives 50 geometries in total. The effects of Rayleigh number (Ra), aspect ratio in addition to the ellipses orientations are investigated. The dynamic and thermal fields as well as the geometry average Nusselt number calculation ($Nu_{avg}=(Nu_{avo}+Nu_{avi})/2$) are analyzed. Nu_{avg} values are ranked at the end in a descending order to show which geometry offers the largest heat exchange rate and *vice versa*, that is something very useful in practice. It should be noted that a good choice of the geometry shape may lead to have a more homogeneous thermal field, a result which goes against the stratifying effect of natural convection that has sometimes to be avoided.

Keywords: Aspect ratio, Concentric ellipses, Heating type, Natural convection, Nusselt number, Rayleigh number.

INTRODUCTION

Heat exchangers have become indispensable industrial equipment for decades. They can provide heating as well as cooling. They can be found in different sizes, from giant ones in nuclear or oil industries to those compact or very small, used in the electrical or electronic fields. In general, they are with circular passage sections, with the possibility of being simple or annular. They can ensure heat

* Corresponding author **Abderrahmane Horimek**: Department of Mechanical Engineering, Ziane Achour University, Djelfa, Algeria; E-mail: Horimek_aer@yahoo.fr

exchange between a fluid and a wall (or walls), as they can be used to ensure heat exchange between two fluids separated by a wall, where circulations in parallel or opposite flows are encountered in practice. Mastering the existing mechanisms during heat transfer in the heat exchanger is, therefore, crucial to better exploit physical, operational (dynamic and thermal) and geometric performances. Doing this is not really easy and must always go through robust calculations that are strongly influenced by growing practical demands. By way of example, previously, the heating process was supposed to be as forced convection (laminar or turbulent-established), where the problem may be of generalized-Graetz, Graetz or completely fully-developed (dynamically and thermally). Whereas, with the industrial progress, more and more complex fluids appeared. One can cite the case of non-Newtonian fluids which have a viscosity strongly influenced by the shear within the fluid; Nanofluids, whose thermal conductivity changes according to percentage, shape and size of the added nanoparticles [1 - 4]. One can also cite the case of thermodependent fluids in viscosity and/or density. When viscosity decreases in hot zones, this leads to a new distribution of velocity and hence temperature as a consequence of the viscosity gradient [5, 6]. The density's thermodependency -which is the source of our proposed work- is often neglected in heat exchangers calculations. Negligence gave underestimation errors during calculations. For this case, a natural convection secondary flow is generated from the entrance section of the heat exchanger tube(s); after a certain distance from the entrance, the secondary flow becomes intense and then no longer negligible, the heating process becomes of mixed convection nature. The corresponding distance is described by the critical Cameron number (X^*). Far downstream, the hot fluid is cumulated at the top and the cold fluid at the bottom, where a clear and unpleasant thermal stratification takes place in a section (Fig. 1). We note that this problem is three-dimensional in nature. To remedy to this thermal stratification, authors of [7, 8] proposed to make an eccentricity between the two pipes of the annular passage, where a downward shift of the inner cylinder revealed a good correction.

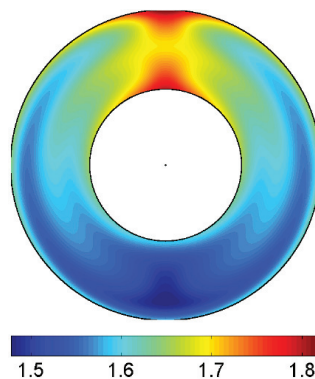


Fig. (1). Thermal stratification in a section.

Based on the details previously given and in order to find a more convenient solution to the original problem, we decided to exploit the geometric parameter of the annular space by proposing the case of natural convection alone but for two concentric ellipses (in the broad sense of an ellipse). The homogeneity of the thermal field will be the main objective sought, but the quantification of the heat exchange rate is also important. It is clear that mainly the thermal distribution obtained in the case of natural convection here, will be obtained in the original case of mixed convection. It is noted that the initial case with circular section duct ($R_1/R_2=0.5$) is also discussed and serves as a witness. In addition, the number of geometries processed here (50 cases) exceeds that found in literature, which provides a positive contribution to the literature. Furthermore, Nu_{avg} (geometry mean Nusselt number) was calculated for each one of them, to better know the cases offering the best rates of heat exchange. Its values are listed in descending order at the end of the results' section.

The fact that the present study deals with the case of two-dimensional natural convection between two concentric ellipses, it will be important to present some close and useful works for the benefit of the work and of the readers. Therefore, among the old works dealing with elliptical annular geometry, we cite the work of M. M. Elshamy *et al.* [9], in which they assumed the case of two concentric horizontal ellipses, where the interior is under high temperature and the exterior under low temperature. Finite volume approach was used for the discretization of the problem equations, rewritten in a curvilinear coordinate system after transformation. Interesting results have been provided for the local and averaged Nusselt, in addition to temperature, streamline and vorticity fields for many considerations. Correlations have been proposed for a narrow range of variation of Ra . The work of J. P. Caltagirone *et al.* [10] can be consulted for the case of two concentric circles, where six geometric cases have been assumed. Since then, a huge number of works have been published, notably with the spectacular advance of computational tools. Among the works close to ours, we cite the work of Y.D. Zhu and *et al.* [11], very rich in a number of assumed geometries. The work is highly recommended, although all results are provided for $Ra=10^4$, $Pr=0.71$ and $AR=2.6$ only. For close and recent works, Tayebi *et al.* [12] studied the problem for the *Cu*-Water nanofluid between two differentially heated concentric horizontal ellipses. In addition to the effects of Ra and the nanoparticles concentration, the authors assumed three eccentricities (Aspect ratio for others) for the hot inner ellipse. The case of an ellipse under imposed flux has been assumed in another study by the same authors [13]. Tayebi and Öztop [14] have shown an improvement in heat exchange when hybrid nanoparticles are used. Another very interesting work which deserves to be consulted for the case of two circles is published by Yang and Kong [15]. In addition to the attractive resolution technique employed (SPH: Smoothed Particle Hydrodynamics), wide ranges of

CHAPTER 8

Theoretical Study of the Geometrical Parameters Effect on the Behavior of a Solar Chimney Power Plant**Haythem Nasraoui^{1,*}, Zied Driss¹ and Hedi Kchaou¹**¹ *Laboratory of Electro-Mechanic Systems (LASEM), National School of Engineers of Sfax (ENIS), University of Sfax (US), 3038 Sfax, Tunisia*

Abstract: Solar Chimney Power Plant (SCPP) is a large scale setup designed for generating green power from the thermal solar energy. In this work, a theoretical SCPP model was developed to study the impact of the main design parameters on the SCPP performance. Based on the Manzanares prototype, the proposed model was verified and validated with the experimental data. The thermodynamic characteristics of the SCPP were analyzed by varying the chimney height, the chimney radius and the collector radius. Results show that the chimney height presents an important effect of the air flow behavior. Otherwise, the proposed model has a good agreement to predict the SCPP performance.

Keywords: Chimney effect, Green energy, SCPP, Solar energy, Theoretical model.

INTRODUCTION

The rise of the pollution rate and the global warming problems around the world led humanity to search for clean and renewable energy resources. Solar Chimney Power Plant (SCPP) is an attractive technology to produce the electrical power from the thermal solar energy. The SCPP is composed of a horizontal solar collector, a tall chimney and a turbine installed at the chimney bottom. The solar radiations pass through the transparent roof of the collector to increase the internal energy of the air under the roof. Thus a hot wind is created inside the system by natural convection to turn the turbine that produces the electrical power. The performance of the SCPP system depends on the design parameters of each component.

* **Corresponding author Haythem Nasraoui:** Laboratory of Electro-Mechanic Systems (LASEM), National School of Engineers of Sfax (ENIS), University of Sfax (US), 3038 Sfax, Tunisia; E-mail: haithem_nasraoui@yahoo.fr

The first prototype was built in Manzanares of Spain by Professor Jorg Schlaich in 1982 [1]. It is characterized by steel chimney of 200 m in height and 244 m of collector diameter. This prototype can generate around 50 kW of overall electrical power [2]. After the experimental validation of the SCPP principle by this prototype, several systematic and theoretical analysis were developed to enhance the overall performance of the SCPP. Basically, the geometrical parameters of the different components were investigated and discussed in several researches. CFD techniques were used widely to analyze the SCPP setup and optimize its design. Ayadi *et al.* [3] investigated the effect of the chimney height on the local SCPP characteristics. They noted that an increase of the chimney height increases the air velocity and thus the kinetic power. Pastohr *et al.* [4] used the commercial ANSYS-Fluent to model a Central geometrically like that of Manzanares to conduct an examination with more details in the description of the operation method and the system performance. Ayadi *et al.* [5] simulated the SCPP system with different turbulence models employed in ANSYS Fluent. Their results show that a standard k- ϵ turbulence model gives an adequate prediction of the SCPP performance. Ayadi *et al.* [6] presented an unsteady state simulation of SCPP coupled with an axial turbine. They observed that the local characteristics of airflow within the turbine vary with the change of the environmental conditions. Bouabidi *et al.* [7] compared several configurations of the chimney based on a small prototype. They changed in each time the venturi location along the chimney. Results show that a divergent solar chimney presents an efficient solution. Also, the impact of the divergent chimney on the overall performance was studied in several works (Hu *et al.* [8, 9]; Xu and Zhou [10]; Hassan *et al.* [11]. Ming *et al.* [12] used a large 3D domain to predict the influence of ambient crosswind on the SCPP performance. They found interesting results which give a realistic behavior of the SCPP system. Kasaeian *et al.* [13] carried out a 3D numerical simulations to show the effect of the turbine blades number on the SCPP performance. Shirvan *et al.* [14] presented an optimization process of the SCPP based on the coupling of the CFD and the experiment plan methods. They found a better tendency of the geometrical parameters effect, but these results are limited to a small scale since they are based on a prototype with 12m in height.

Otherwise, analytical modeling presents an efficient tool to predict the SCPP performance. Several mathematical models were conducted in the last few decades to evaluate the global performance of SCPP. For instance, Weinrebe *et al.* [15] present a simple theoretical model for assessing the difference between the Solar Chimney power plant and a Down-Draught energy Tower. Zhou *et al.* [16] studied the effect of the chimney height and collector size on the power generating system using a simple mathematical model. They varied the collector radius from 1 m to 4 m and the chimney height from 1 m to 8 m. Their study confirms that the power output increases as the chimney height and the collector

radius increase. By varying the solar radiation intensity from 500 to 1000 W.m⁻², they proved that the power output grows as the solar radiation intensity increases. Ming *et al.* [17] offered a comprehensive model to evaluate the performance of a SCPP, based on the resolve of the static pressure, driving force and the power output. Li *et al.* [18] developed an analytical model of solar chimney to predict the optimal pressure drop of the turbine. Ming *et al.* [19] developed various mathematical models for the solar collector, the chimney and the energy storage layer in order to assess the effect of solar radiation on the heat storage characteristic. Ming *et al.* [20] presented a thermodynamic analysis on the solar chimney power plant and advanced energy utilization degree to analyze the performance of the system. Later, Bernardes *et al.* [21] presented a mathematical model to define the thermal compartment and the generated power performance of a large scale of a solar chimney power plant. At the same context, Koonsrisuk [22] presented a mathematical model based on the continuity, the momentum, the energy, and the state equations for the sloped solar chimney setups. Their work focused on the performance of the sloped solar chimney. Hurtado *et al.* [23] analyze the thermodynamic behavior of a solar chimney power plant over a daily operation cycle with considering the soil as a heat storage system. They studied the influence of the soil thermal inertia and the effects of soil compaction degree on the output power generation. The analysis proved that the output power increases by 10% as the soil compaction increases. Nizetic *et al.* [24] analyzed the potential for electric energy production in Mediterranean countries. In their work, they estimated the quantity and price of the generated energy. Their work proved that solar chimney power plant is an efficient solution for Mediterranean countries. Pasumarthi and Sherif [25] established the most used model which combined the effects of the chimney, the turbine, the single and double canopy, the ground storage materials and the ambient cross wind. Hamdan [26] highlighted that the chimney height, the collector radius and the turbine pressure drop are essential parameters for the SCPP design. Gholamalizadeh *et al.* [27] analyzed the buoyancy-driven flow field and the heat transfer inside the SCPP based on the greenhouse effect. Li *et al.* [28] studied the SCPP system taking account the effects of heat and flow losses and the temperature lapse rate inside and outside of the chimney. They demonstrated that the foundation of the turbine in the SCPP system reduces power output.

In this chapter, a novel analytical model is developed to evaluate the performance of solar chimney power plant and optimizing its different dimensions. Compared to the literature, the presented model is characterized by its simplicity and its few input data. The optimization process took into account the thermodynamic characteristics of the air. In fact, geometrical parameters such as collector diameter, collector height, chimney height and chimney diameter were optimized. Manzanares model was adopted as a reference case in this chapter.

Numerical Investigations of the Effect of Packed Bed Porosity on the Flow Behavior

Hajer Troudi^{1,*}, Moncef Ghiss¹, Mohamed Ellejmi² and Zoubeir Tourki^{1,3}

¹ Laboratoire de Mécanique de Sousse (LMS), Ecole Nationale d'Ingénieurs de Sousse (ENISo), 4023 Sousse, Université de Sousse, Sousse, Tunisie

² Alpha Engineering International (AEI), Sousse, Tunisie

³ LMS ENISo-Université de Sousse, Directeur de la Mission Universitaire de Tunisie en Allemagne, Godesberger Allee 103, 53175 Bonn, Germany

Abstract: Packed columns are considered useful to a great extent in the distillation of natural gas, and liquid volume fraction is a critical parameter for their design. This study aimed to develop a geometrical model of a packed column with one cone spray to simulate the injection. Here, the commercial software FLUENT 6.3 was employed. CFD simulations using the mixture model coupled with several turbulence models were used to analyze the porosity effect on the fluid profiles. The results show that the decrease of the packed porosity resulted in a greater dispersion of the liquid, indicating the anisotropic behavior in the bed. Furthermore, the effect of different turbulence models was analyzed in order to study the atomizing of the liquid phase accurately. The numerical results were obtained to provide further insight into the mechanism of the distillation with volatile components.

Keywords: CFD, Distillation, ICEM, Liquid Volume Fraction, Mixture Model, Packed Bed, Porosity, Spherical Particles, Spray, Turbulence.

INTRODUCTION

Packed bed reactors are used for the distillation or combustion of chemical hydrocarbons [1, 2]. Unlike the widespread technologies of packed systems [3, 4], most studies have focused on random ones [5]. To have an optimal design, several parameters, such as porosity, packing diameter, and the ratio between the packed bed length and the packing diameter, are of crucial importance for the fluid flow selectivity. In particular, porosity has attracted more and more attention in recent years, and therefore, the goal of this paper was to analyze the porosity effect on the fluid profiles.

* Corresponding author Hajer Troudi: Laboratoire de Mécanique de Sousse (LMS), Ecole Nationale d'Ingénieurs de Sousse (ENISo), 4023 Sousse, Université de Sousse, Sousse, Tunisie; E-mail: Hajer.Troudi@eniso.u-sousse.tn

So far, several numerical and experimental studies about the porosity effect on the behavior of fluid have been found in the literature. These studies used the computational fluid dynamics (CFD) as a powerful tool for the investigation. Gupta *et al.* [6] studied the dynamics of the irregular packings near the wall of a fixed bed. Guo *et al.* [7] used a large packing of equal size but different ratio values.

They concluded that the fluid velocity increases sharply in the axial and radial directions of the packed bed. Wu *et al.* [8] worked on small packing diameters of about 0.1 to 0.6 mm. It was demonstrated that heat, mass transfer, and the velocity within the bed were significantly dependent on the shape and size of the particles. Moreover, most available packed systems contain only one single cone spray placed on the top of the bed. The reason behind that is to minimize the computational cost and to increase the mesh resolution. Du *et al.* [9] highlighted the benefit of using one single cone spray. At fixed porosity, they investigated the gas-liquid interaction in the interstitial spaces between the particles. They provided a further in-depth understanding of the transport phenomenon on the particle scale since it affects the performance of the packed bed.

Among the numerous approaches of CFD (*e.g.*, Euler-Lagrange, Euler-Euler, VOF, and Mixture), in the present study, the fourth one is employed to study the transient-state flow inside the packed bed at different porosity values. The packed bed is treated as porous media, and an additional term of Ergun pressure drop correlation is implemented in the Navier-Stokes equations. In addition, we evaluated the influence of turbulence models on the liquid distribution in order to assess the appropriate model.

METHOD

The geometry and the grids for the computational domain are created using ICEM CFD, and the simulations are performed in ANSYS Fluent 14.5. The details of numerical models, column geometry, mesh generation, as well as the choice of the optimal mesh, convergence criteria, and simulation conditions are discussed in the following subsections. Conclusions are drawn in the final section.

Packed Column Process

Fig. (1) shows a typical packed column used in petrochemical industries that contains two packing beds, two distributor plates for the liquid phase, and different inlet-outlet nozzles. The feed of the liquid phase is introduced from the top of each plate distribution, sprayed by gravity through the spray cones to the down of the column, and then discharged into the outlet nozzle. On the other side, the gas phase is moved from the bottom to the top of the column through nozzles.

The packed column is formed by random spherical packings of diameter d_ϵ (m) and a void fraction ϵ (-). In order to simplify the model and due to the symmetry of the system, a single stage of packed bed with one cone-spray is adopted for modelling in Ansys Fluent, as shown in Fig. (1).

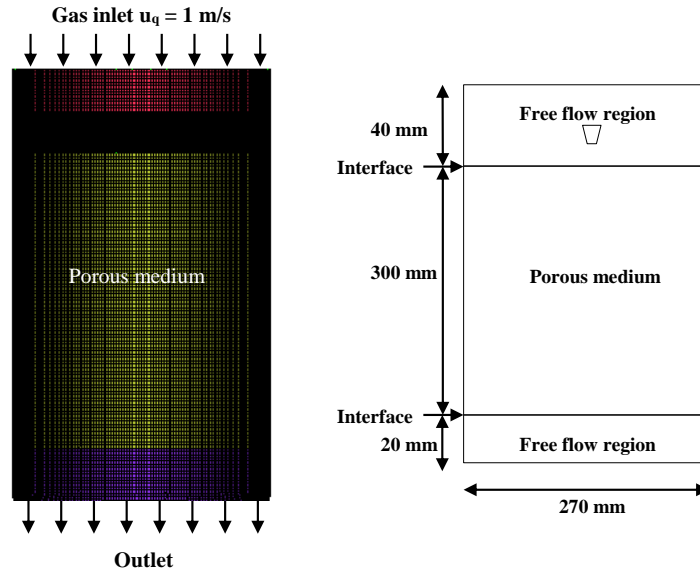


Fig. (1). (a) Computational grid and boundary condition (b) grid detail near the nozzle-spray and (c) the frontal view.

Governing Equations

The equations detailed below are applicable to the mixture multiphase model in which the gaseous phase is defined as the primary carrier phase and denoted by the subscript q while the liquid phase is defined as the secondary dispersed phase and denoted by the subscript p . The simulations are performed using Ansys Fluent [10]. The balance equations are derived in mass-weighted average form and given as below:

$$\frac{\partial(\alpha_p \rho_p)}{\partial t} + \nabla \cdot (\alpha_p \rho_p \mathbf{u}_m) = -\nabla \cdot (\alpha_p \rho_p (\mathbf{u}_p - \mathbf{u}_m)) + \dot{m}_{qp} - \dot{m}_{pq} \quad (1)$$

$$\begin{aligned} \frac{\partial(\rho_m \mathbf{u}_m)}{\partial t} + \nabla \cdot (\rho_m \mathbf{u}_m \mathbf{u}_m) = & -\nabla p_m + \nabla \cdot (\overline{\boldsymbol{\tau}_m}) + \rho_m \mathbf{g} + \mathbf{F}_m \\ & + \nabla \cdot \left(\sum_{k=1}^2 (\alpha_k \rho_k (\mathbf{u}_p - \mathbf{u}_m) (\mathbf{u}_p - \mathbf{u}_m)) \right) \end{aligned} \quad (2)$$

Comparison between a Conventional and a Four-Stage Savonius Wind Rotor

Sobhi Frikha^{1,*}, Zied Driss¹ and Mohamed Salah Abid¹

¹ *Laboratory of Electro-Mechanic Systems (LASEM), National Engineering School of Sfax (ENIS), University of Sfax, 3038 Sfax, Tunisia*

Abstract: In this study, the influence of the shape on the characteristics of a Savonius wind rotor was studied in numerical simulations and experimental measurements. Particularly, we compared the features of the Savonius rotor with a new design rotor consisting of a four-stage configuration. We used “Solid Works Flow Simulation” to display the local characteristics in various transverse and longitudinal planes. The Navier-Stokes equations and the standard k- ϵ turbulence model were solved in the numerical model. A finite volume discretization method was applied to solve these equations. The experimental measurements were conducted in an open wind tunnel to validate the numerical model.

Keywords: CFD, Savonius rotor, Turbulent flow, Wind tunnel.

INTRODUCTION

With the increasing scarcity of fossil fuels, the demand for renewable energy sources is increasing, mainly wind energy which is becoming the most efficient technology for power production. Savonius wind turbines are a type of vertical-axis wind turbine, rotating because of the drag force generated by the blades. Some of the best features of savonius wind turbines are their simplicity, efficiency and low noise generation. Some works have been done to improve the design of the Savonius rotor. Grinspan *et al.* [1] designed a new blade shape with a twist. A maximum power coefficient of 0.5 was obtained. Menet and Bourabaa [2] examined the effect of some parameters on the characteristics of the flow around a Savonius rotor, such as the overlap ratio, the shaft, the chassis and the Reynolds number. Numerical results were compared to the experimental ones. Saha *et al.* [3] performed experiments with a different number of stages. They noticed that the rotor displays improved performance characteristics as the number of stages

* **Corresponding author Sobhi Frikha:** Laboratory of Electro-Mechanic Systems (LASEM), National Engineering School of Sfax (ENIS), University of Sfax, 3038 Sfax, Tunisia; E-mail: frikha_sobhi@yahoo.fr

rises from one to two. Nevertheless, the performance decreases when the number of stages was equal to three. Mohamed *et al.* [4] improved the design of a Savonius turbine with two and three blades to increase the output power. Other authors such as D'Alessandro *et al.* [5], Dobрева and Massouh [6], Zhou and Rempfe [7], carried out numerical simulations in order to compare the improved design of Savonius rotors to the others. Roy *et al.* [8] concluded that the efficiency of a Savonius rotor can be increased considerably by selecting the correct numerical method.

Kamoji *et al.* [9] studied the effect of the Reynolds number on a modified Savonius rotor without a shaft. The power coefficient rises by 19 percent when the number of Reynolds rises from 80,000 to 150,000. Akwa *et al.* [10] investigated the effect of the buckets overlap ratio on the torque and power coefficients. The highest efficiency was obtained for buckets overlap ratios close to 0.15. Khan *et al.* [11] tested different blade profiles of a Savonius rotor for different values of the overlap. Driss *et al.* [12] performed a numerical study of the flow around an incurved Savonius rotor. They compared the results with the experimental ones obtained in a wind tunnel. Compared to a circular rotor, the flow circulation of the incurved rotor is improved. Sharma *et al.* [13] studied a two-stage Savonius rotor with 2 blades. They conducted experiments and studied different parameters like the overlap, the tip speed ratio, the power and the torque coefficient. A maximum power coefficient of 0.517 was obtained at 9.37% overlap. In addition, power and torque coefficients decreased when the overlap increased.

According to these previous findings, it is very important to investigate the design of the Savonius wind rotor in order to enhance the efficiency of the rotor. In this context, we were interested in studying the shape effect on the flow around a Savonius rotor. Indeed, we compared the numerical results in the case of a single – stage and a four-stage Savonius rotor having the same height $H=200$ mm. The experiments were also conducted in an open wind tunnel, and the experimental data were compared with our numerical results. The experimental data recorded in this work contain corrections for wind tunnel blockage.

GEOMETRY SYSTEM

Savonius Wind Rotor

In this work, we were interested in a Savonius vertical-axis wind turbine. The rotor consists of a Plexiglas bucket with a height $H = 200$ mm, a diameter $D = 173$ mm, an aspect ratio $H/D = 1.15$ and an overlap ratio $m/D = 0.034$ (Fig. 1). An AM-4204 anemometer has been used to determine the wind speed at various locations with an accuracy of 0.1 m/s (Fig. 2). We have used a digital tachometer

CA-27 to measure the rotational speed of the turbine rotor, as presented in Fig. (3). A DC generator was used to calculate the dynamic torque exerted on the rotor shaft, converting the torque into an electric current. The generator is coupled to the dynamometer RZR-2102 model. Fig. (4) presents the four-stage Savonius rotor assembled with the dynamometer.

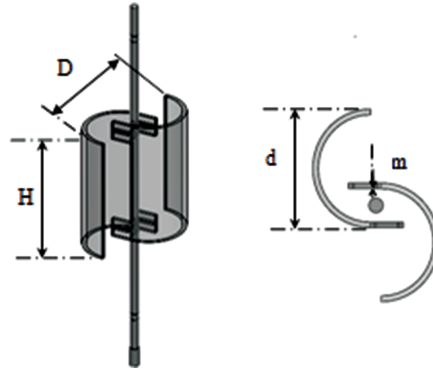


Fig. (1). Vertical axis savonius semi-circular.

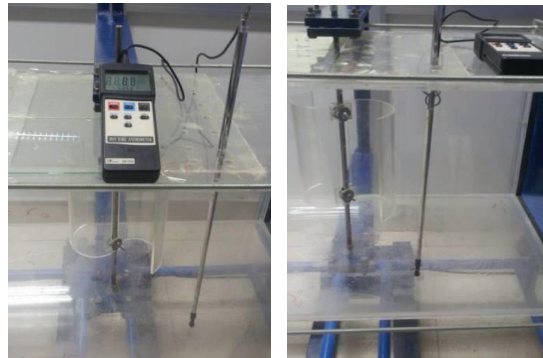


Fig. (2). Anemometer.



Fig. (3). Tachometer.

SUBJECT INDEX**A**

Absorber 48
 thermal 48
 Acceleration, gravity 149
 Agriculture crop drying 49
 Agro-food micro-enterprises 47
 Air 22, 24, 47, 48, 49, 50, 54, 85, 89, 90, 92,
 93, 108, 109, 131, 132, 133, 134, 135,
 141, 142
 atmospheric 132, 134
 density 132, 135
 flow 48, 132
 flux 49, 50
 gap membrane distillation (AGMD) 22
 pollution 85
 solar collector 54
 Air collector 47, 48
 thermal 48
 Airflow 48, 49, 130, 132
 double pass 48, 49
 single-pass 49
 Algorithm, genetic 31
 Analysis 2, 81, 131
 thermal 2, 81
 thermodynamic 131
 Angle 38, 49, 50, 62, 67, 108, 111
 azimuthal 111
 burning 67
 clearance 38
 Annand's correlation 73
 Artificial 31, 32, 33
 intelligence resources 33
 neural networks 31, 32

B

Behavior 131, 146, 171
 aerodynamic 171
 anisotropic 146
 thermodynamic 131
 Burn fraction 69

C

Calculations 40, 51, 63, 70, 75, 88, 91, 105,
 106, 138, 160
 geometry average Nusselt number 105
 heat exchangers 106
 theoretical 63
 Canopy, double 131
 Centrifugal forces 14
 CFD 130, 154
 method 154
 techniques 130
 Chaotic motion 14
 Characteristic(s) 7, 53, 54, 68, 129, 131, 140,
 141, 142, 143
 aerodynamic airflow 140, 141, 142
 electrical Power-Voltage 53, 54
 gas constant 68
 global airflow 143
 thermodynamic 129, 131
 thermophysical 7
 Chimney 129, 130, 131, 132, 134, 135, 136,
 137, 142
 divergent 130
 steel 130
 effect 129
 inlet 132, 135
 pipe 136, 142
 section 132
 Chimney radius 129, 138, 142
 effect 142
 CO₂ pollutants 100
 Coefficients, skin friction 2, 14
 Collector 133, 161, 165
 air 133
 inlet 161, 165
 Collector radius 129, 130, 131, 138, 141, 143
 effect 141
 Combustion 1, 62, 63, 64, 66, 68, 71, 74, 75,
 76, 77, 78, 80, 84, 85, 89, 90, 91, 92, 93,
 95, 97, 98, 99, 100, 102
 adiabatic 89, 95

chamber 64, 69, 74, 76, 77, 78
 compression ignition 62
 efficiency 66, 71, 100
 engines 1, 63
 for constant pressure 91
 process 62, 63, 65, 68
 products 80, 85, 89, 90, 92, 93, 99
 quality 76
 systems 84
 temperatures calculus 97
 velocity 75
 Competitive market environment 30
 Components, microelectronic 1
 Computational 130, 146, 148, 147, 150, 156
 fluid dynamics (CFD) 130, 146, 147, 150, 156
 grid and boundary condition 148
 Conditions 27, 53, 56, 63, 72, 81, 85, 97, 100, 102, 130, 140, 160
 climate 85
 environmental 130
 hydrodynamic fluid 27
 stoichiometric 63, 72, 100
 Conductivity, thermal 3, 4, 7, 49
 Consumption, fuel mass 65
 Convection 1, 10, 16, 74, 106, 110, 118
 forced 1, 10, 16, 106
 heat exchange 118
 heat transfer 74, 110
 Crank angle 64, 76, 78
 burning duration 76
 function of 64, 78
 Customizable tools 74
 Cylinder pressure 62, 63, 64, 66, 69, 73

D

Density's thermodependency 106
 Dichotomy method 97
 Digital tachometer 157
 Dimensionless governing equation 109
 Direct contact membrane distillation (DCMD) 22
 Distribution 107, 161, 162
 thermal 107
 velocity field 161, 162
 Drilling 31, 33, 35, 39, 40
 elementary reduced 40
 machines 33
 Dynamic 15, 118

agitation 118
 benefits 15

E

Effects, porosity 146, 147
 Efficiency 3, 47, 138
 cooling 3
 energetic 47
 turbine generation 138
 Electric connectivity 47
 Electrical 47, 48, 49, 50, 52, 53, 54, 55, 56, 57
 efficiencies 47, 48, 52, 54, 56, 57
 energies 47, 50
 performance 47, 49, 52, 53, 54, 55
 Ellipses 105, 107, 108, 110, 112, 113, 118, 119, 120, 121, 123, 124, 126
 cold 112
 outer 123
 Energy 14, 21, 48, 67, 85, 86, 111, 131, 141
 chemical 67
 kinetic 86
 mechanical 85
 renewable 48
 Energy production 47, 57, 84, 131
 electric 131
 electrical 47
 thermal 47
 Engine 60, 61, 62, 63, 65, 66, 67, 69, 70, 71, 74, 75, 76, 79, 80, 81
 explosion stroke 70
 genset dual-fuel diesel 61

F

Flame 75, 76, 84, 85, 86, 87, 91, 98, 101, 102
 development 76
 diffusion 86, 87, 101
 development period 76
 propagation periods 76
 Flow sensitivity 149
 Fluid 21, 106, 123, 147
 heating 123
 thermodependent 106
 velocity 21, 147
 Fluid motion 115, 116, 121
 disturbance 121
 Flux, cooling 3
 Force 39, 47, 131, 149, 151, 156
 drag 156

driving 131
 gravitational 151
 thrust 39
 Forced convection coefficient 133
 Fossil fuels 84, 85, 156
 burning 84
 Four-stage Savonius rotor 157, 158, 162, 163,
 164, 165, 167, 168
 Fuel 60, 61, 62, 63, 68, 72, 75, 84, 85, 86, 87,
 90, 91, 98, 99, 100, 102
 air equivalence ratio and stoichiometry 90
 burned 98
 changing 63
 combustible 63
 consumption 84, 85, 87, 99, 100, 102
 gaseous 61
 hydrocarbon 62
 natural 85

G

Gas 1, 21, 23, 25, 28, 63, 64, 68, 80, 85, 146,
 151, 154
 flushing 25
 greenhouse 85
 natural 146
 produced greenhouse 85
 storage 23
 turbines 1, 85
 Gibbs function 101
 Glass fiber 50
 Greenhouse effect 85, 131

H

Heat 47, 49, 66, 72, 75, 76, 78, 89, 116, 131
 recovering 47
 recovering waste 49
 sensible 89
 transferring 116
 release 66, 75, 76, 78
 release rate 72
 storage system 131
 Heat transfer 1, 2, 3, 9, 10, 21, 22, 64, 67, 73,
 76, 110, 113
 activity 3
 properties 2, 3
 Heat transfer coefficient 3, 54, 63, 65, 78, 80,
 133, 138
 conductive 133

Heating process 106, 132, 142

I

Industrial progress 106
 Industries 1, 4, 32, 48, 105, 113, 147
 electrical 4
 food 1
 oil 105
 petrochemical 147
 Inert gas 21, 23, 25, 27, 28
 flow of 25, 27
 velocity 21, 25, 28
 Influence 25, 54, 85
 direct 25
 growing 85
 of solar radiation 54
 Injection 2, 72
 nanofluid jet 2
 systems 72
 Inlet 2, 149
 jet 2
 radius 149
 Inner 121, 122
 horizontal ellipses 121
 vertical ellipses 122
 Inner ellipse 107, 123
 hot 107
 Isomorphism 32
 Isotherms and stream-functions 112

J

Jets 2, 4, 8, 14
 confined air 2

K

Kerosene-air 98, 101
 and methane-air combustion 98
 combustion 98, 101

L

Liquid distribution 147, 151
 calculated 151
 Liquid volume 150
 distribution function 150
 Liquid volume fraction 146, 150, 153, 154

- profiles 150
- M**
- Mass 22, 26, 27, 57, 60, 65, 66, 91, 95, 149, 154
 - conservation law 95
 - density 149
 - flow rates influence 57
 - fraction 60, 65, 66, 91, 149, 154
 - transfer coefficient 26, 27
 - transfer mechanisms 22
- Material(s) 39, 44
 - collision 44
 - database 39
- Matlab software 21
- Mean 34, 70
 - effective pressure 70
 - square error learning 34
- Membrane distillation 21, 22
 - gas scavenging 21
- Mesh independence test 9
- N**
- Nanofluid(s) 1, 2, 3, 4, 7, 9, 12, 15, 16, 106, 108
 - properties 7
 - viscosity 7
 - water 3, 9
- Nanoparticle(s) 14
 - shapes, cylindrical 14
 - volume friction 14
- Natural convection intensification 113
- Navier-Stokes equations 147, 156, 159
- Network 31, 32, 34, 35
 - architectures 31
 - nonlinearity 32
 - processing 32
 - stability 34
- Neurons 32, 34
 - biological 32
 - output 32
- Newtonian fluid 105, 108
- Newton's law 74
- Nonlinear equations 92
- O**
- Outer 118, 125, 126
 - circle/inner horizontal ellipse 118
 - horizontal ellipse/Inner circle 118, 125, 126
- Outer and inner 121, 122
 - horizontal ellipses 121
 - vertical ellipses 122
- Outputs, thermal 47, 50
- Oxygen concentration 61
- P**
- Permeate fluxes 23, 28
- Photovoltaic 47, 48
 - thermal collector 48
- Polynomial equation 135, 136, 137
- Porous media 147
- Pressure 24, 27, 61, 62, 64, 68, 69, 70, 75, 76, 77, 78, 88, 131, 135, 137, 149, 150, 160, 161, 164, 165
 - atmospheric 137, 150
 - dynamic 135, 165
 - intake 62
 - losses, friction 135
 - outlet 160
 - prediction function 64
 - static 131, 135, 137, 164
 - theoretical 70
- Production, pollutant 100
- Products 47, 49, 84, 89, 90, 91, 93, 98, 99, 102, 132
 - agricultural 47
 - agro-food 49
 - global thermodynamic 132
- Propagation, flame front 62
- Properties 2, 7, 85
 - thermodynamic 85
 - thermophysical 2, 7
- R**
- Rayleigh number 105, 109, 113
- Reaction 84, 101, 102
 - endothermic 102
 - enthalpies of 84, 101
- Reverse osmosis (RO) 22
- Reynolds 1, 3, 12, 156, 157, 160
 - number 1, 12, 156, 157, 160
 - turbulent jet 3
- RNA applications 31

S

Savonius 157, 160
 rotor geometries 160
 turbine 157
Scavenging gas membrane distillation (SGMD) 21, 22, 24, 25, 26, 27, 28
Simulations, thermodynamic 62, 63
Soil compaction 131
Solar 48, 49, 51, 57
 heating 49
 irradiance 51
 thermal 49
Solar chimney 130, 131
 divergent 130
 sloped 131
Solar collector 55, 129
 horizontal 129
 prototype 55
Solar energy 47, 48, 57, 129
 thermal 129
 conversion 48
Solar radiation 47, 50, 51, 52, 53, 54, 56, 131, 132, 141
 global incident 51
 intensity 52, 131
Stoichiometric proportions 91
System, transmission 32

T

Tachometer 158
Technologies 22, 30, 48, 129, 146
Thermal 3, 47, 48, 49, 50, 51, 54, 57, 63, 70, 85, 110, 113, 114, 121, 123, 131, 132, 139
 comportment 131
 conditions 110, 113, 114, 121, 123
 efficiency 3, 48, 49, 50, 51, 54, 57, 63, 70, 139
 energy 47, 49, 50, 54, 85, 132
Thermization process 127
Thermodynamic(s) 60, 67, 69, 84, 88
 equilibrium condition 88
 first law of 60, 67, 69, 84
Torque, dynamic 158, 171
Transient-state flow 147
Transitional flows 159
Translational motion 64
Turbine 131, 135, 136, 138

 machinery efficiency 138
 pressure 131, 135, 136, 138
Turbulence energy 6, 159
Turbulent kinetic energy 6, 153, 166, 167

V

Vacuum membrane distillation (VMD) 22
Vortex effect 75

W

Wall boundaries 160
Waschni's correlation 63
Water vapour pressure 24
Wiebe function 60, 63, 64, 65, 66, 69, 72
Wind 156, 157, 159, 160, 171
 energy 156
 tunnel 156, 157, 159, 160, 171
 tunnel components 159
Woschni's model 60



Zied Driss

Prof. Zied Driss is a full-time Professor in the Department of Mechanical Engineering at the National School of Engineers of Sfax (ENIS). He received his Engineering Diploma in 2001, his Master Degree in 2003, his Ph.D. in 2008, and his HDR in 2013 in Mechanical Engineering from ENIS at the University of Sfax, Tunisia.

He is interested in developing numerical and experimental techniques for solving problems in mechanical engineering and energy applications. Also, his research has been focused on the interaction between Computational Fluid Dynamics (CFD) and Computational Structure Dynamics (CSD) codes. As a result of his research, he is the principal or co-principal investigator on more than 250 papers in peer-reviewed journals, more than 500 communications to international conferences, 30 books, and 80 books chapters. Also, he is the main inventor of 12 patents. Currently, Prof. Driss is a Team Leader in the Laboratory of Electromechanical Systems (LASEM), an Editorial Board Member and reviewer for different international journals, an Editor for different books, a General Chair of two bi-annual international conferences, and an active member in different national and international associations.